A statistical mechanical theory of proton transport kinetics in hydrogen-bonded networks based on population correlation functions with applications to acids and bases

ARTICLE *in* THE JOURNAL OF CHEMICAL PHYSICS · SEPTEMBER 2010

Impact Factor: 2.95 · DOI: 10.1063/1.3474625 · Source: PubMed

3 AUTHORS, INCLUDING:

Mark E Tuckerman
New York University
182 PUBLICATIONS **13,099** CITATIONS

SEE PROFILE

A statistical mechanical theory of proton transport kinetics in hydrogen-bonded networks based on population correlation functions with applications to acids and bases

Mark E. Tuckerman, Amalendu Chandra, and Dominik Marx

Citation: J. Chem. Phys. **133**, 124108 (2010); doi: 10.1063/1.3474625
View online: http://dx.doi.org/10.1063/1.3474625
View Table of Contents: http://jcp.aip.org/resource/1/JCPSA6/v133/i12
Published by the American Institute of Physics.

A statistical mechanical theory of proton transport kinetics in hydrogen-bonded networks based on population correlation functions with applications to acids and bases

Mark E. Tuckerman,[1,a)] Amalendu Chandra,[2,b)] and Dominik Marx[3,c)]
[1]*Department of Chemistry and Courant Institute of Mathematical Sciences, New York University, New York, New York 10003, USA*
[2]*Department of Chemistry, Indian Institute of Technology, Kanpur 208016, India*
[3]*Lehrstuhl für Theoretische Chemie, Ruhr-Universität Bochum, 44780 Bochum, Germany*

(Received 31 March 2010; accepted 12 July 2010; published online 30 September 2010)

Extraction of relaxation times, lifetimes, and rates associated with the transport of topological charge defects in hydrogen-bonded networks from molecular dynamics simulations is a challenge because proton transfer reactions continually change the identity of the defect core. In this paper, we present a statistical mechanical theory that allows these quantities to be computed in an unbiased manner. The theory employs a set of suitably defined indicator or population functions for locating a defect structure and their associated correlation functions. These functions are then used to develop a chemical master equation framework from which the rates and lifetimes can be determined. Furthermore, we develop an integral equation formalism for connecting various types of population correlation functions and derive an iterative solution to the equation, which is given a graphical interpretation. The chemical master equation framework is applied to the problems of both hydronium and hydroxide transport in bulk water. For each case it is shown that the theory establishes direct links between the defect's dominant solvation structures, the kinetics of charge transfer, and the mechanism of structural diffusion. A detailed analysis is presented for aqueous hydroxide, examining both reorientational time scales and relaxation of the rotational anisotropy, which is correlated with recent experimental results for these quantities. Finally, for OH^-(aq) it is demonstrated that the "dynamical hypercoordination mechanism" is consistent with available experimental data while other mechanistic proposals are shown to fail. As a means of going beyond the linear rate theory valid from short up to intermediate time scales, a fractional kinetic model is introduced in the Appendix in order to describe the nonexponential long-time behavior of time-correlation functions. Within the mathematical framework of fractional calculus the power law decay $\sim t^{-\sigma}$, where σ is a parameter of the model and depends on the dimensionality of the system, is obtained from Mittag–Leffler functions due to their long-time asymptotics, whereas (stretched) exponential behavior is found for short times. © *2010 American Institute of Physics*.
[doi:10.1063/1.3474625]

I. INTRODUCTION

Proton transfer (PT) along hydrogen bonds (HBs) is a ubiquitous phenomenon underlying a great variety of molecular processes ranging from chemistry to physics and biology.[1] For instance, any acid or base catalyzed chemical reaction requires PT among the elementary steps.[2] Charge migration is also instrumental in fuel cells, wherein charge (usually hydronium or hydroxide ions) must be transported through aqueous pores in polymeric membranes[3] or through various types of anhydrous materials.[4,5] In biology, vectorial PT is often among the primary chemical events, for example, at the beginning of signal transduction cascades.[6] Unraveling the microscopic mechanisms of PT and, more importantly, true long-range and long-time proton transport in multidimensional HB network topologies, is critical for understanding and controlling such processes. These processes are not only mediated by protons, H^+, but also by "proton holes" resulting in the transport of negative charge as carried by OH^- species.[7,8] Although the same simple principle of such nonvehicular or structural diffusion proposed by von Grotthuss more than 200 years ago underlies most PT and charge transport processes in HB media,[9] the specific local solvation pattern including the crucial fluctuations that govern the mechanism varies from system to system. Among other things this leads to qualitatively different structural diffusion scenarios when it comes to negative versus positive charge defects migrating in bulk water, which implies distinctly different charge transport mechanisms in bases and acids.[7,8]

Theoretically, *ab initio*,[9] semiempirical,[10] and reactive force-field[11] molecular dynamics simulations have been able to elucidate many details of the dominant solvation complexes and mechanisms of structural diffusion associated with topological defects in a large variety of HB systems. This includes the charge migration mechanism of solvated

[a)]Electronic mail: mark.tuckerman@nyu.edu.
[b)]Electronic mail: amalen@iitk.ac.in.
[c)]Electronic mail: dominik.marx@rub.de.

OH^- defects in bulk water,[7,12–16] $OH^-(aq)$, which is now known to differ qualitatively from the related $H^+(aq)$ system.[7,8,15,16] Despite these successes, however, the problem of consistently extracting lifetimes of these complexes as well as the exchange times and rates of charge transport from molecular dynamics remains a challenge because PT reactions cause the identity of the core of a structural defect in the HB network to change continually. The introduction of a theoretical framework capable of delivering these properties would be especially timely as ultrafast spectroscopic measurements[17–25] are revealing new details about elementary PT steps, solvation patterns, charge transport, and various associated ultrashort time scales.

In this paper, we lay out a general statistical mechanical theory that achieves the aforementioned goals. The theory employs a set of indicator or population functions for locating defect structures in HB networks, including their particular solvation topologies and their associated time correlation functions, which can be computed directly from a molecular dynamics trajectory. The decay behavior of these correlation functions encodes the desired relaxation times, lifetimes, and rates. Using these correlation functions as the basis of a chemical master equation framework[26–29] provides a means whereby these quantities can be extracted by fitting the decay pattern to the solution of the posited kinetic model. The basic machinery of population time-correlation functions[30,31] and associated rate equations[32–35] is well-established and is now considered a standard tool in the analysis of HB kinetics.[33–41] Here, however, we show how to rework this formalism to treat PT and subsequent charge transport kinetics along the lines of our earlier publications on this issue.[16,42] We investigate the various types of such correlation functions that are usually defined, i.e., intermittent and continuous, and show that these can be related by a simple integral equation formalism. We then proceed to solve the integral equation iteratively and provide a graphical interpretation of the iterative solution. By applying the theory to the two archetype problems of charge defect transport, i.e., the hydrated proton, $H^+(aq)$, and the hydroxide ion, $OH^-(aq)$, in bulk water we show that direct links exist between the defect's dominant solvation structures, the kinetics of charge transfer, and the mechanism of structural diffusion for each case. Moreover, by separating out simple proton "rattling" events, in which a proton simply shuttles forth and back in a HB, from true charge displacement events, we show that the theory is capable of extracting time scales and rates associated with both processes. The linear theory discussed so far, which describes the kinetics for short to intermediate time scales, is generalized within the framework of fractional kinetics, thereby extending the validity of the approach (see Appendix). In particular, the intermittent PT correlation function is expressed in fractional kinetics in terms of a superposition of Mittag–Leffler functions, which feature (stretched) exponential and algebraic decay at short and long-times, respectively.

This paper is organized as follows: In Sec. II A, we define the indicator functions and their associated time correlation functions. We then explore different types of kinetic models for the decay of these correlation functions, and we derive and analyze the solutions of these models. In Sec. II B, we go deeper into the theory of correlation functions by relating several of them from Sec. II A via an integral equation. We obtain an iterative solution to this equation and give the solution a graphical interpretation. The current knowledge on the structure, dynamics, and kinetics of hydronium and hydroxide charge defects in liquid water is introduced in Sec. III A and the computational details underlying this study are reviewed in Sec. III B. In Sec. IV, we present applications of our theory using *ab initio* molecular dynamics[43] (AIMD) trajectories of $H^+(aq)$ and $OH^-(aq)$ in Secs. IV A and IV B, respectively, where we show that this linear chemical master equation approach is capable of connecting charge transport kinetics to underlying molecular mechanisms in each case. The "dynamical hypercoordination" mechanism proposed to describe the delicate interplay of the solvation patterns and charge migration of $OH^-(aq)$ is shown in Sec. IV C to be consistent with all available experimental data and thus governs the behavior of hydroxide ions in aqueous environments, in particular, in basic solutions. Finally, in the Appendix, we suggest that the linear rate theory, which leads to exponential decay of the correlation functions, can be generalized to nonexponential long-time behavior within a framework based on fractional kinetics.

II. CONCEPTS AND THEORETICAL FRAMEWORK

A. Population correlation functions and solvation-shell dynamics

We begin by introducing some nomenclature and the definitions of the indicator functions to be employed in the theory. For simplicity, we will consider systems in which HB donors/acceptors are the same chemical species A, i.e., $A-H\cdots A$, although all ideas are easily generalized to heterogeneous $A-H\cdots B$ systems. When a positively or negatively charged topological defect is created by the addition or removal of a proton, respectively, there is always a structural defect site, for which the HB donor or acceptor will be denoted by A^*. Note that A^* will either have an excess or missing proton, depending on whether the defect is cationic, e.g., $H^+(aq)$ or anionic, e.g., $OH^-(aq)$. We now define[16] two charge defect indicator or population functions, $h(t)$ and $H(t)$, to monitor PT as a function of time as follows: $h(t)=1$ if a tagged A atom is A^* at time t [and $h(t)=0$ otherwise], and $H(t)=1$ if A^* retains its identity *continuously* in the time interval $[0,t]$. In addition, we define a third indicator function $g(t)$ such that $g(t)=1$ if a given atom A is in the first solvation-shell of A^* (but not equal to A^*) at time t, and it is 0 otherwise.

Based on these defect population functions, in Ref. 16, we introduced a set of time correlation functions, which have a probabilistic interpretation, with the aim of rigorously describing the dynamics and structural diffusion of charge defects in hydrogen-bonded networks. We now review the definitions of these correlation functions. We first introduce an "intermittent" PT correlation function[16] defined to be

$$C_i(t) = \frac{\langle h(0)h(t)\rangle}{\langle h\rangle}. \tag{1}$$

These correlation functions are also called "history-independent" or "memory-independent" in the literature. This correlation function yields the probability that an atom A that was A^* at $t=0$ will become A^* at t, irrespective of any identity changes that occur in the interim. Note that the same function, called the history independent pair correlation function $c(t)$, was subsequently used as the basis of a nonlinear kinetics model for proton diffusion.[44] The analogous "continuous" (i.e., "history-dependent" or "memory-dependent") PT correlation function[16]

$$C_c(t) = \frac{\langle h(0)H(t)\rangle}{\langle h\rangle} \tag{2}$$

gives the probability that an atom A that was A^* at $t=0$ will remain as A^* up to time t. The importance of the continuous correlation function is that it can be used to calculate the A^* lifetime, τ_{exch}, from

$$\tau_{exch} = \int_0^\infty C_c(t)dt, \tag{3}$$

with τ_{exch} being a measure of the time associated with a PT event from A^* to a first solvation-shell molecule. Finally, we introduce the nearest-neighbor correlation function[16]

$$C_{nn}(t) = \frac{\langle h(0)g(t)\rangle}{\langle h\rangle}, \tag{4}$$

which provides the probability that if a given atom is A^* at $t=0$, it is in the first solvation-shell of a new A^* at time t irrespective of the location of the defect and its first solvation-shell in the interim. The function $C_{nn}(t)$ is, therefore, also a history-independent correlation function. This new A^* must clearly be in the first solvation-shell of the original A^*.

In calculating the correlation functions in Eqs. (1), (2), and (4), it is important to decide if so-called proton rattling events[9] should be included or excluded. A rattling event is one in which two successive PTs return the proton to the original A^*. Including them allows ultrafast dynamics available in femtosecond measurements[20] to be extracted. However, since these events do not contribute to the overall net displacement of charge, i.e., to transport, excluding them leads to time scales and rates associated entirely with the actual charge transport process.

The decay of the correlation functions in Eqs. (1), (2), and (4) encodes the kinetics of the charge transport process in their temporal behavior. One way of extracting these quantities is via a model of this kinetics. Let us first consider a simple kinetic model of the chemical master equation type.[26–29] Let $[A^*]$ denote the concentration of defect sites and $[A']$ denote the concentration of defect first solvation-shell sites and let B denote any other site in the HB network. A PT reaction transforms A^* into an A' site, and we assume that this reaction can occur in either the forward or backward direction as an equilibrium

$$A^* \rightleftharpoons A'. \tag{5}$$

Furthermore, let k_1^{PT} and k_{-1}^{PT} denote the forward and backward rate constants, respectively. In addition, an A' site can be transformed into a B site by a PT reaction with a forward rate constant k_2^{PT} or through diffusion into the second solvation-shell, which is also described here, in the spirit of Ref. 45, by a rate equation with a rate constant k_2^D. Since B is not in the first solvation-shell of A^*, we can only consider these as forward processes with a combined rate constant k_2,

$$A' \rightarrow B, \tag{6}$$

so that $k_2 = k_2^{PT} + k_2^D$. If we assume first-order kinetics, we can introduce the following rate equation corresponding to reaction (5):

$$\frac{d[A^*](t)}{dt} = -k_1^{PT}[A^*](t) + k_{-1}^{PT}[A'](t). \tag{7}$$

The population correlation functions $C_i(t)$ and $C_{nn}(t)$ can now be interpreted as prescribing average fractional occupations of defect and first solvation-shell sites and, therefore, we can recast Eq. (7) as

$$\frac{dC_i(t)}{dt} = -k_1^{PT}C_i(t) + k_{-1}^{PT}C_{nn}(t). \tag{8}$$

If we take $C_i(t)$ and $C_{nn}(t)$ directly from a molecular dynamics simulation and use Eq. (8) to fit the rate constants k_1^{PT} and k_{-1}^{PT}, then any long-time purely diffusional contribution is automatically included. However, if we use reaction (6) to "close" the set of rate equations, then we obtain

$$\frac{d[A'](t)}{dt} = -(k_2 + k_{-1}^{PT})[A'](t) + k_1^{PT}[A^*](t) \tag{9}$$

or

$$\frac{dC_{nn}(t)}{dt} = -(k_2 + k_{-1}^{PT})C_{nn}(t) + k_1^{PT}C_i(t). \tag{10}$$

Equations (8) and (10) constitute a chemical master equation, which predicts purely exponential decay of the populations as we will now show.

The solution of Eqs. (8) and (10) for the two unknown correlation functions $C_i(t)$ and $C_{nn}(t)$ yields a biexponential form for both correlation functions. This can be readily seen by taking the Laplace transform of both first-order differential equations. Using the notation

$$\tilde{f}(s) = \int_0^\infty e^{-st}f(t)dt \tag{11}$$

for the Laplace transform of a function $f(t)$, we obtain the following two equations:

$$\begin{aligned} s\tilde{C}_i(s) - 1 &= -k_1^{PT}\tilde{C}_i(s) + k_{-1}^{PT}\tilde{C}_{nn}(s), \\ s\tilde{C}_{nn}(s) &= -K\tilde{C}_{nn}(s) + k_1^{PT}\tilde{C}_i(s), \end{aligned} \tag{12}$$

where $K = k_2 + k_{-1}^{PT}$ and we have used the fact that $C_i(0)=1$ and $C_{nn}(0)=0$. Eliminating $\tilde{C}_{nn}(s)$ from the algebraic equations, we find that $\tilde{C}_i(s)$ becomes

$$\tilde{C}_i(s) = \frac{s+K}{(s+k_1^{PT})(s+K) - k_1^{PT}k_{-1}^{PT}}. \quad (13)$$

Since the denominator is a quadratic function of s, the inverse Laplace transform, which picks up both poles of $\tilde{C}_i(s)$, must contain two exponentials. Moreover, it is straightforward to show that the poles are both real and negative, implying biexponential decay. Inverting the Laplace transform gives the following form for the intermittent PT correlation function:

$$C_i(t) = \frac{1}{2\lambda}[(\lambda - k_1^{PT} + K)e^{-(k_1^{PT}+K-\lambda)t/2} + (\lambda + k_1^{PT} - K)e^{-(k_1^{PT}+K+\lambda)t/2}], \quad (14)$$

where

$$\lambda = \sqrt{(k_1^{PT}-K)^2 + 4k_1^{PT}k_{-1}^{PT}}. \quad (15)$$

According to Eq. (14), $C_i(t)$ contains a slow decay component $\exp[-(k_1^{PT}+K-\lambda)t/2]$ with weight $a_{slow}=(\lambda-k_1^{PT}+K)/2\lambda$ and a fast decay component $\exp[-(k_1^{PT}+K+\lambda)t/2]$ with weight $a_{fast}=(\lambda+k_1^{PT}-K)/2\lambda$. If we fit $C_i(t)$ to a general biexponential form

$$C_i(t) = a_0 e^{-a_1 t} + (1-a_0)e^{-a_2 t}, \quad (16)$$

then the relation between the parameters a_0, a_1, and a_2 and the rate constants is[42]

$$k_1^{PT} = a_1 a_2 + a_2(1-a_0),$$

$$k_{-1}^{PT} = \frac{(a_1-a_2)^2 a_0(1-a_0)}{a_0 a_1 + a_2(1-a_1)}, \quad (17)$$

$$k_2^{PT} = \frac{a_1 a_2}{a_1 a_0 + a_2(1-a_0)}.$$

The corresponding nearest-neighbor correlation function $C_{nn}(t)$ can be readily obtained as

$$C_{nn}(t) = \frac{k_1^{PT}}{\lambda}[e^{-(k_1^{PT}+K-\lambda)t/2} - e^{-(k_1^{PT}+K+\lambda)t/2}], \quad (18)$$

which contains the same slow and fast decay components. In terms of the fitting parameters, this correlation function is written as

$$C_{nn}(t) = \frac{a_0 a_1 + a_2(1-a_0)}{a_1 - a_2}[e^{-a_2 t} - e^{-a_1 t}]. \quad (19)$$

Note that in the limit of $k_{-1}^{PT} \gg k_2$, $C_i(t)$ shows a single exponential decay with a time constant equal to $(k_1^{PT}+k_{-1}^{PT})^{-1}$,

$$C_i(t) = \frac{k_1^{PT}}{k_1^{PT}+k_{-1}^{PT}} e^{-(k_1^{PT}+k_{-1}^{PT})t} + \frac{k_{-1}^{PT}}{k_1^{PT}+k_{-1}^{PT}}. \quad (20)$$

The decay of $C_{nn}(t)$ in this limit is given by

$$C_{nn}(t) = \frac{k_1^{PT}}{k_1^{PT}+k_{-1}^{PT}}[1 - e^{-(k_1^{PT}+k_{-1}^{PT})t}] \quad (21)$$

so that the equilibrium or the long-time ratio of the two probabilities is given by the ratio of the forward and backward rate constants as expected.

The PT correlation functions in Eqs. (1), (2), and (4) inherently assume that there is only one fundamental solvation pattern associated with the defect. An important aspect of structural diffusion problems, however, is that the defect site might support *several* solvation patterns with qualitatively *different* HB coordination numbers. Suppose that there are p such patterns each with a different coordination number $n_1, \ldots, n_j, \ldots, n_p$. If we wish to predict the lifetime of a given coordination state, then we need to modify the continuous PT correlation function $C_c(t)$ in such a way that different solvation patterns are accounted for separately. Accordingly, we now introduce the PT correlation function $C_c^{(n_j)}(t)$ capable of distinguishing between the different patterns with the definition[16]

$$C_c^{(n_j)}(t) = \frac{\langle h_{n_j}(0)H(t)\rangle}{\langle h_{n_j}\rangle}, \quad (22)$$

where $h_{n_j}(t)$ is 1 if a given tagged atom is A^* at time t with coordination number n_j and 0 otherwise. Thus, $C_c^{(n_j)}(t)$ measures the probability that a tagged atom remains A^* continuously up to time t given that its coordination number is n_j at $t=0$. The lifetime $\tau_{exch}^{(n_j)}$ of the solvation pattern is then given by

$$\tau_{exch}^{(n_j)} = \int_0^\infty C_c^{(n_j)}(t)dt. \quad (23)$$

We note that one can also calculate the correlation function $\langle h(0)H_{n_j}(t)\rangle/\langle h\rangle$ which would give the probability that a given coordination pattern is retained continuously up to time t. This correlation function can decay through PT and also through HB breaking/forming without necessarily involving any PT. Hence, its dynamics would not necessarily capture the PT rates alone. Since, in the present work, we are interested in extracting the rates of PT events starting from different hydrogen bonding states, the function $C_c^{(n_j)}(t)$ appears to be more relevant in the present context.

In addition, we introduce a pattern-specific version $C_{nn}^{(n_j)}(t)$ of $C_{nn}(t)$ as[16]

$$C_{nn}^{(n_j)}(t) = \frac{\langle h_{n_j}(0)g(t)\rangle}{\langle h_{n_j}\rangle}, \quad (24)$$

such that $C_{nn}^{(n_j)}(t)$ measures the probability that if a given atom is A^* at time $t=0$ with coordination number n_j, it will be in the first solvation-shell of a new A^* at time t. Finally, we could also define an analogous intermittent or history-independent correlation function $C_i^{(n_j)}(t)$ as the probability that if a given atom A is A^* at $t=0$ with coordination number n_j, it is also A^* at time t; however, we will not make explicit use of such a function. If each $C_{nn}^{(n_j)}(t)$ has an associated backward rate constant $k_{-1,j}^{PT}$, the complete set of rate equations becomes

$$\frac{dC_{\rm i}(t)}{dt} = -k_1^{\rm PT}C_{\rm i}(t) + \sum_j k_{-1,j}^{\rm PT}C_{\rm nn}^{(n_j)}(t),$$
$$\frac{dC_{\rm nn}^{(n_j)}(t)}{dt} = -(k_2^{\rm PT} + k_{-1,j}^{\rm PT})C_{\rm nn}^{(n_j)}(t) + k_1^{\rm PT}C_{\rm i}(t). \quad (25)$$

In order to see how the existence of additional solvation patterns affects the dynamics, let us consider the case of $p=2$ distinct solvation complexes, which is relevant for analyzing the OH^-(aq) scenarios. For this case, the chemical master equation set becomes

$$\frac{dC_{\rm i}(t)}{dt} = -k_1^{\rm PT}C_{\rm i}(t) + k_{-1,1}^{\rm PT}C_{\rm nn}^{(n_1)}(t) + k_{-1,2}^{\rm PT}C_{\rm nn}^{(n_2)}(t),$$
$$\frac{dC_{\rm nn}^{(n_1)}(t)}{dt} = -(k_2 + k_{-1,1}^{\rm PT})C_{\rm nn}^{(n_1)}(t) + k_1^{\rm PT}C_{\rm i}(t), \quad (26)$$
$$\frac{dC_{\rm nn}^{(n_2)}(t)}{dt} = -(k_2 + k_{-1,2}^{\rm PT})C_{\rm nn}^{(n_2)}(t) + k_1^{\rm PT}C_{\rm i}(t).$$

Taking Laplace transforms of these equations gives

$$s\tilde{C}_{\rm i}(s) - 1 = -k_1^{\rm PT}s\tilde{C}_{\rm i}(s) + k_{-1,1}^{\rm PT}\tilde{C}_{\rm nn}^{(n_1)}(s) + k_{-1,2}^{\rm PT}\tilde{C}_{\rm nn}^{(n_2)}(s),$$
$$s\tilde{C}_{\rm nn}^{(n_1)}(s) = -K_1\tilde{C}_{\rm nn}^{(n_1)}(s) + k_1^{\rm PT}\tilde{C}_{\rm i}(s), \quad (27)$$
$$s\tilde{C}_{\rm nn}^{(n_2)}(s) = -K_2\tilde{C}_{\rm nn}^{(n_2)}(s) + k_1^{\rm PT}\tilde{C}_{\rm i}(s),$$

where $K_1=k_2+k_{-1,1}^{\rm PT}$ and $K_2=k_2+k_{-1,2}^{\rm PT}$. Eliminating the two nearest-neighbor correlation functions and solving for $\tilde{C}_{\rm i}(s)$ yields, after some algebra

$$\tilde{C}_{\rm i}(s) = \frac{(s+K_1)(s+K_2)}{(s+k_1^{\rm PT})(s+K_1)(s+K_2) - k_1^{\rm PT}k_{-1,1}^{\rm PT}(s+K_2) - k_1^{\rm PT}k_{-1,2}^{\rm PT}(s+K_1)}. \quad (28)$$

In general, since the denominator in Eq. (28) is cubic, there will be three poles, all real and negative, giving rise to a tri–exponential decay.

We note that the bi- or *multiexponential* decay behavior of the intermittent PT correlations that is found in the above analysis originates from the use of *linear* rate equations with *first-order* rate constants for different decay channels. As will be demonstrated in Sec. IV, this approach is valid in the present context, especially over short and intermediate times, since the decay of the intermittent PT correlations at such time scales primarily occurs through structural diffusion which can indeed be described by PT rate constants. The contribution of slower hydrodynamic diffusion is expected to be small in the decay of PT correlations. If there is a contribution from hydrodynamic diffusion, it is expected to influence the PT correlation functions only at long-times, i.e., beyond the time scales considered in Sec. IV for our numerical calculations; nonexponential kinetics of long-time HB relaxation is a well-known and well-studied phenomenon in pure water.[33–35,46,47] Indeed, the *biexponential* decay scenario derived for proton transport kinetics in Ref. 16 as applied therein to AIMD trajectories and analyzed above has been confirmed explicitly in Ref. 44 to describe the decay of the intermittent/history-independent PT correlation function very accurately up to $t' \approx 30$ ps, where it is already decayed to about 5% of its initial value, i.e., $c(t')/c(0) \approx 0.05 \ll 1/e$. Only beyond about 30 ps do the deviations from biexponential decay become noticeable when $c(t)$ is analyzed on a double-logarithmic scale: $c(100\ \text{ps})/c(0) \approx 5\times10^{-3}$ from empirical valence bond MD simulation versus $c(100\ \text{ps})/c(0) \approx 1\times10^{-4}$ from the biexponential fit; these estimates of $c(t)$ are extracted from Fig. 6 of Ref. 44. The current simulation results for $C_{\rm i}(t)$, to be described in Sec. III, are also found to follow a decay pattern described by a biexponential form for the hydrated proton and a triexponential form for the hydrated hydroxide ion over a time interval of approximately 8 ps with correlation coefficients for the fit to these forms exceeding 0.98.

In order to account for such long-time effects,[33–35,46,47] a nonlinear kinetic theory was introduced in Ref. 44 to describe proton migration kinetics on a time scale of ~100 ps. This was achieved by extending reversible geminate recombination theory as applied to HB kinetics in pure water[47] via the introduction of a distance- and temperature-dependent diffusion coefficient $D(r)$ into the Laplacian and using PT correlation functions as introduced in Ref. 16. The nonlinear distance dependence is obtained, using a phenomenological model, from the time-variation of the diffusion constant $D(t)$ as obtained from a nonlinear three-parameter fit to the relative mean-square displacements obtained at each temperature from empirical valence bond MD simulations. The resulting multiparameter kinetic model extends the simple three-parameter biexponential form, Eq. (16), obtained from linear kinetics beyond 30 ps and successfully describes the algebraic decay properties of $c(t) \sim t^{-3/2}$ for time scales on the order of 100 ps as demonstrated in Fig. 5 of Ref. 44. In the Appendix, we consider an alternative mathematical framework to predict such power law behavior of intermittent PT correlation functions at long-times using the concept of fractional kinetics.

B. Integral equation formalism connecting intermittent and continuous correlation functions

We now seek to establish a direct connection between the decay properties of the intermittent/history-independent

and continuous/history-dependent PT correlation functions. In order to establish this connection, we first recognize that the intermittent correlation function $C_i(t)$ must be an upper bound to the continuous correlation function. Therefore, in the extreme limit that there is no change of identity of A^* in the interval $[0,t]$, we have $C_i(t)=C_c(t)$. In addition, if we define probability densities associated with the intermittent and continuous correlation functions as

$$c_i(t) = -\frac{dC_i}{dt},$$
$$c_c(t) = -\frac{dC_c}{dt}, \tag{29}$$

then to lowest order $c_i(t)=c_c(t)$. A reduction from the upper bound occurs when there is a PT event in the interval $[0,t]$ that changes the location of the defect in the HB network. In order to incorporate this, we define a probability $N_c(t)$ as the probability that if an atom A is A^* for $t<0$, it remains a nearest-neighbor of A^* continuously in the interval $[0,t]$ before it becomes A^* again at time t.

The probability density associated with $N_c(t)$

$$n_c(t) = -\frac{dN_c}{dt}. \tag{30}$$

This definition of $N_c(t)$ is sufficient to describe rattling events. However, if we wish to treat long-range charge transport, then $N_c(t)$ should be generalized to be the probability that an atom A that ceased to be A^* at $t=0$ does not become A^* again during the interval $[0,t]$. Note that by construction, for either definition, a product of the form $n_c(t_3-t_2)n_c(t_2-t_1)=0$, for $t_3>t_2>t_1$, as it would require that an atom be both A^* and a first neighbor of A^* for some period time in the interval $[t_1,t_3]$, which is not possible. The probability is again increased if two PTs bring the defect back to the original A^*.

Given these facts, we can now write down an integral equation of the Volterra type satisfied by the intermittent correlation function density as

$$c_i(t) = c_c(t) - \int_0^t dt' n_c(t-t')c_i(t') + \int_0^t dt' \int_0^{t'} dt'' c_c(t-t')n_c(t'-t'')c_i(t''). \tag{31}$$

Since n_c and c_c are both continuous probability densities, we take these to be small compared to $c_i(t)$. Hence, we can treat the second term on the right in Eq. (31) as a first-order term and the third term as second order. This classification will help us in the proceeding analysis as we develop an iterative solution to Eq. (31). Note that by defining a kernel $K(t_1,t_2)$ as

$$K(t_1,t_2) = n_c(t_1)\delta(t_2) - c_c(t_1)n_c(t_2), \tag{32}$$

Eq. (31) can be written more compactly as

$$c_i(t) = c_c(t) - \int_0^t dt' \int_0^{t'} dt'' K(t-t',t'-t'')c_i(t''). \tag{33}$$

We now derive an iterative solution to Eq. (31). We start with the zeroth order solution $c_i^{(0)}(t)=c_c(t)$. The first-order solution is now obtained by substituting this zeroth order solution into the first-order term and dropping the second-order term. Thus,

$$c_i^{(1)}(t) = c_c(t) - \int_0^t dt_1 n_c(t-t_1)c_i^{(0)}(t_1) = c_c(t) - \int_0^t dt_1 n_c(t-t_1)c_c(t_1). \tag{34}$$

We now take this first-order solution and feed it back into Eq. (31) to obtain a second-order solution

$$c_i^{(2)}(t) = c_c(t) - \int_0^t dt_1 n_c(t-t_1)c_i^{(1)}(t_1) + \int_0^t dt_1 \int_0^{t_1} dt_2 c_c(t-t_1)n_c(t_1-t_2)c_i^{(0)}(t_2), \tag{35}$$

which simplifies to

$$c_i^{(2)}(t) = c_c(t) - \int_0^t dt_1 n_c(t-t_1)c_c(t_1) + \int_0^t dt_1 \int_0^{t_1} dt_2 c_c(t-t_1)n_c(t_1-t_2)c_c(t_2). \tag{36}$$

This process can be repeated *ad infinitum* to generate the entire series. At third order and higher, for example, we obtain

$$\begin{aligned} c_i(t) = c_c(t) &- \int_0^t dt_1 n_c(t-t_1)c_c(t_1) \\ &+ \int_0^t dt_1 \int_0^{t_1} dt_2 c_c(t-t_1)n_c(t_1-t_2)c_c(t_2) \\ &- \int_0^t dt_1 \int_0^{t_1} dt_2 \int_0^{t_2} dt_3 n_c(t-t_1)c_c(t_1-t_2)n_c(t_2-t_3) \\ &\times c_c(t_3) + \cdots. \end{aligned} \tag{37}$$

The series has a particularly interesting form in the Laplace space. Taking the Laplace transform of the series yields

$$\begin{aligned} \tilde{c}_i(s) &= \tilde{c}_c(s) - \tilde{n}_i(s)\tilde{c}_c(s) + \tilde{c}_c(s)\tilde{n}_c(s)\tilde{c}_c(s) \\ &\quad - \tilde{n}_c(s)\tilde{c}_c(s)\tilde{n}_c(s)\tilde{c}_c(s) + \cdots \\ &= \tilde{c}_c(s)[1 + \tilde{n}_c(s)\tilde{c}_c(s) + \tilde{n}_c(s)\tilde{c}_c(s)\tilde{n}_c(s)\tilde{c}_c(s) + \cdots] \\ &\quad - \tilde{n}_c(s)\tilde{c}_c(s)[1 + \tilde{n}_c(s)\tilde{c}_c(s) \\ &\quad + \tilde{n}_c(s)\tilde{c}_c(s)\tilde{n}_c(s)\tilde{c}_c(s) + \cdots] \\ &= \frac{\tilde{c}_c(s)[1-\tilde{n}_c(s)]}{1-\tilde{n}_c(s)\tilde{c}_c(s)}, \end{aligned} \tag{38}$$

where the fact that the series in square brackets is a geometric series and can be summed analytically has been used. Equations (37) and (38) are similar to those obtained by Luzar[35] in the context of HB dynamics; however, to our

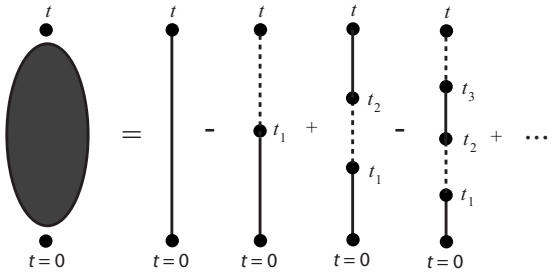

FIG. 1. Graphical representation of Eq. (37).

knowledge, the underlying integral equation, Eq. (31), has not appeared previously.

We can give the solution for $c_i(t)$ the following graphical interpretation: Let the time points $0, t_1, t_2, \ldots, t$ be the vertices of a graph, let each factor of c_c be represented by a solid edge, and let each factor n_c be represented by a dashed edge. Then each term in the series of Eq. (37) can be represented by a graph in which the vertices are connected by an alternating pattern of solid and dashed edges, with the first edge always being a solid edge for the leading factor of c_c. The graphical representation of the series solution of Eq. (31) is shown in Fig. 1. On the left, $c_i(t)$ is represented as an abstract process in which what occurs between $t=0$ and t is unknown since the defect is unobserved between these two end points.

Now let us consider a simple example in which $C_c(t)$ and $N_c(t)$ are described by single exponential decay. In this case, the corresponding probability densities are given by

$$\tilde{c}_c(s) = \frac{k_1^{PT}}{s + k_1^{PT}}, \tag{39}$$

$$\tilde{n}_c(s) = \frac{k_{-1}^{PT}}{s + k_{-1}^{PT} + k_2}. \tag{40}$$

The form of $\tilde{n}_c(s)$ comes from noting that $n_c(t)$ describes the continuous probability density of A′ remaining as A′ from time 0 to t before it decays to A* and not to B in the bulk. Substituting Eqs. (39) and (40) in Eq. (38), we obtain the following expression for the intermittent probability density:

$$\tilde{c}_i(s) = \frac{k_1^{PT}(s + k_2)}{s^2 + s(k_1^{PT} + k_{-1}^{PT} + k_2) + k_1^{PT}k_2}. \tag{41}$$

The two roots of the denominator of the right hand side of the above equation are

$$s_\pm = \tfrac{1}{2}[-(k_1^{PT} + k_{-1}^{PT} + k_2) \pm \sqrt{(k_1^{PT} + k_{-1}^{PT} + k_2)^2 - 4k_1^{PT}k_2}]. \tag{42}$$

Noting that

$$\sqrt{(k_1^{PT} + k_{-1}^{PT} + k_2)^2 - 4k_1^{PT}k_2} = \sqrt{(k_1^{PT} - k_{-1}^{PT} - k_2)^2 + 4k_1^{PT}k_{-1}^{PT}} = \lambda$$

[as defined by Eq. (15)], the two roots can be re-expressed as

$$s_\pm = -\tfrac{1}{2}[k_1^{PT} + k_{-1}^{PT} + k_2 \pm \lambda], \tag{43}$$

which give a biexponential decay of $C_i(t)$ with identical time constants as given by Eq. (14). We again note that in the limit of $k_{-1}^{PT} \gg k_2$, $C_i(t)$ exhibits a single exponential decay profile: $C_i(t) \sim \exp[-(k_1^{PT} + k_{-1}^{PT})t]$. When $C_c(t)$ and $N_c(t)$ are biexponential functions of the forms $C_c(t) \sim A\exp[-\lambda_1 t] + (1-A)\exp[-\lambda_2 t]$ and $N_c(t) \sim B\exp[-\lambda_3 t] + (1-B)\exp[-\lambda_3 t]$ with $\lambda_2 \gg \lambda_1$ and $\lambda_4 \gg \lambda_3$, then the algebra to show that $C_i(t)$ is also biexponential is considerably more involved. However, by plotting $\tilde{c}_i(s)$ using Eq. (38), as is done in Fig. 2(a), it is clear that $\tilde{c}_i(s)$ has two poles, indicating that $c_i(t)$ and $C_i(t)$ are both biexponential functions as well. The same can be seen in Fig. 2(b), which shows if triexponential forms for $C_c(t)$ and $N_c(t)$ are input, $\tilde{C}_i(s)$ has three poles and, therefore, $C_i(t)$ is also a triexponential function.

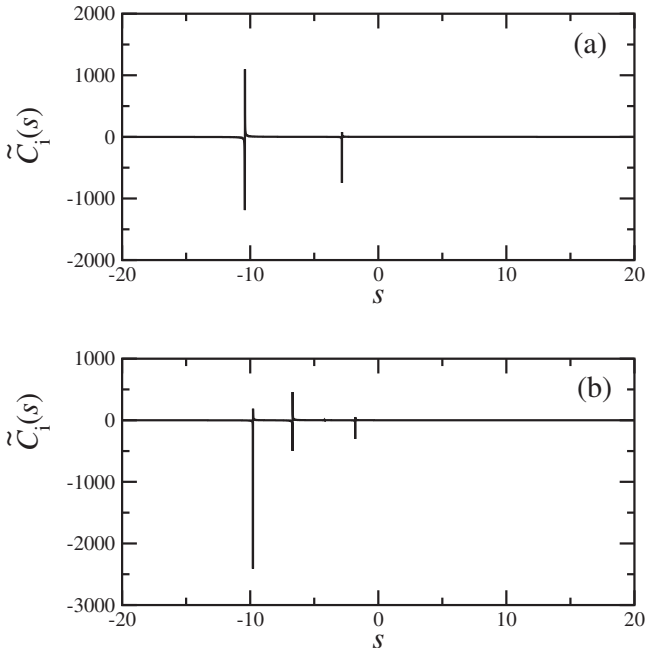

FIG. 2. Laplace transforms of the intermittent correlation function derived from Eq. (38). (a) $C_c(t)$ and $N_c(t)$ are both biexponential functions $C_c(t) = a_0\exp[-a_1 t] + (1-a_0)\exp[-a_2 t]$ and $N_c(t) = b_0\exp[-b_1 t] + (1-b_0)\exp[-b_2 t]$ with $a_0=0.3$, $b_0=0.5$, $a_1=0.25$, $a_2=6.0$, $b_1=0.35$, and $b_2=7.0$. (b) $C_c(t)$ and $N_c(t)$ are both triexponential functions $C_c(t) = a_0\exp[-a_1 t] + A_0\exp[-a_2 t] + (1-a_0-A_0)\exp[-a_3 t]$ and $N_c(t) = b_0\exp[-b_1 t] + B_0\exp[-b_2 t] + (1-b_0-B_0)\exp[-b_3 t]$ with $a_0=0.3$, $A_0=0.4$, $b_0=0.5$, $B_0=0.41$, $a_1=0.25$, $a_2=3.0$, $a_3=6.0$, $b_1=0.35$, $b_2=4.1$, and $b_3=9.1$.

III. SHOWCASE APPLICATIONS

A. Hydronium and hydroxide ions in bulk water

The above formalism will be applied to shed light on the formerly controversial problem[7,13–16,48–52] of OH^- solvation and transport in aqueous solution; see a recent review[8] for the current status. However, because of its direct bearing on $OH^-(aq)$, we test the technique first using the related problem of $H^+(aq)$ solvation and transport in water. The reason for this choice is twofold. First of all, the mechanistic details underlying charge transport in acids are now well understood based on simulations[9] and can be found in textbooks on Physical Chemistry.[53] Second, all essential elements including time scales have been confirmed experimentally[20] using femtosecond vibrational pump-probe spectroscopy.

The $H^+(aq)$ picture[13,14,54] involves an interplay between a threefold coordinated complex known as the "Eigen cat-

ion," $H_3O^+ \bullet (H_2O)_3$, and a shared-proton complex, $[H_2O \cdots H \cdots OH_2]^+$, called the "Zundel cation."[9] Their interconversion is driven by specific fluctuations in the local HB network,[13,14,54] which can be rationalized in terms of the "presolvation concept,"[15] as explained in Refs. 7 and 8. At its core is the common notion that bulk water molecules prefer essentially a fourfold tetrahedral coordination shell subject to fluctuations and defects.[55] More importantly, structural diffusion requires that in any PT reaction, the *proton-receiving* species must first have a solvation pattern that corresponds to the species into which it will be transformed as a result of the reaction. Application to $H^+(aq)$ leads to a picture in which a HB between the first and second solvation-shells of H_3O^+ breaks,[13,14,54] thereby reducing the coordination number of a (proton-receiving) water molecule in the first shell from four to three.[56] The predicted Grotthuss mechanism[13,14,54] was subsequently confirmed experimentally[20] via femtosecond vibrational spectroscopy. A third aspect of the mechanism is the prediction that $H^+(aq)$ cannot be characterized entirely in terms of either the Eigen or Zundel structures due to quantum zero-point motion, but approaches these "idealized" structures only as limiting forms and, therefore, the notion of a "fluxional complex" was coined.[56] This view has also been born out by the measured kinetics[20] obtained from time-resolved ultrafast spectroscopy. Furthermore, it should be noted that the picture just described may be refined by including more solvation-shells[25,57,58] in the spirit of the Eucken–Gierer–Wirtz theory,[59,60] which is derived from a cluster-type view of liquid water. Finally, a more recent AIMD study[61] of the hydrated proton using a converged basis set approach suggests that true structural diffusion events involve a concerted mechanism in which the coordination number reduction in the first solvation-shell must be accompanied by a coordination number increase of the hydronium from three to four as the proton is transferred in order to ensure that the back transfer does not occur.

In stark contrast to $H^+(aq)$, the mechanistic picture of aqueous OH^- transport has been much less clear and has become controversial[7,12–16,48–52] as reviewed in Ref. 8. At first sight, there would appear to be a "mirror symmetry" between $OH^-(aq)$ and $H^+(aq)$: hydronium, H_3O^+, is a water molecule with an excess proton whereas hydroxide, OH^-, is a H_2O with a missing proton, i.e., a "proton hole." According to such ideas, structural diffusion of $OH^-(aq)$ is driven by the same type of second solvation-shell effects that drive $H^+(aq)$ migration.[48]

From AIMD simulations using three popular density functionals, BLYP,[62,63] HCTH 120,[64] and PW91,[65] three different $OH^-(aq)$ solvation patterns and transport mechanisms have been obtained, all of which can be understood using the presolvation concept.[7,8,16] In the following we sketch the three mechanisms in words and refer to the original publications[7,16] for both full detail and pictorial renderings.

The pioneering AIMD studies[12–14] suggested that the oxygen in OH^- is on the average "hypercoordinated"[15] by preferentially *accepting four* HBs in a roughly square-planar arrangement. This peculiar aspect has been confirmed recently by several independent AIMD simulation studies.[66–68] The initial step of the dynamical hypercoordination mechanism[15] is a coordination number reduction of $OH^-(aq)$ itself by breaking a HB between its oxygen and a *first shell* H_2O. Next, this $OH^-(aq)$ *donates transiently one* HB via its hydroxide hydrogen. At this stage, $OH^-(aq)$ finds itself in a locally tetrahedral solvation environment such that the proton can be easily transferred, thus transforming OH^- into an intact H_2O. Concurrently, the donated HB strengthens and leaves the nascent H_2O molecule with two accepted and two donated HBs as required for an ideally coordinated bulk water molecule. According to the dynamical hypercoordination mechanism predicted by the BLYP functional, the rate-limiting step is the time needed for the coordination change in the *first* shell and the relaxation into a tetrahedral configuration.

Using the HCTH functional, the solvation-shell of $OH^-(aq)$ is also predicted to be hypercoordinated, however in a rigid, static way. Thus, in the "static hypercoordination" mechanism, the oxygen of $OH^-(aq)$ accepts four H_2O via HBs in a square-planar arrangement but preserves this coordination such that it cannot receive another proton via PT. Consequently, OH^- behaves like any inert anion with a tightly bound first solvation-shell, $[OH^- \bullet (H_2O)_n](aq)$, and the only possibility to diffuse is that the second solvation-shell changes due to HB fluctuations in the third shell and beyond. This implies that diffusion mostly occurs hydrodynamically via the vehicular Stokes mechanism, whereas PT and thus structural Grotthuss diffusion steps would be rare within the static hypercoordination mechanism.

Finally, in the "mirror image" mechanism[52] obtained by using the PW91 functional, the OH^- hydrogen donates a HB but favors threefold coordination of its oxygen. This implies that OH^- is already solvated tetrahedrally—like any intact water molecule on average. In this arrangement, a proton is readily transferred to this OH^- from an accepted H_2O in the first solvation-shell. Being shifted to the respective neighboring site, the OH^- is again perfectly coordinated and receives in turn a proton from a neighboring H_2O that donates a HB. This mirror image mechanism, as predicted by the PW91, functional yields an extraordinarily high structural diffusion rate.[52]

B. Computational details

AIMD trajectories have been obtained from the well-known PW91,[65] BLYP,[62,63] and HCTH/120 (Ref. 64) functionals. All simulations were performed using the Car–Parrinello technique[43,69–71] and the CPMD code,[70,72] a 9.865 Å periodic cubic box with one OH^- (or H_3O^+) ion and 31 (32 for pure bulk water) H_2O molecules. For the BLYP and HCTH/120 functionals, Troullier–Martins pseudopotentials with a cutoff of 70 Ry were employed and ultrasoft pseudopotentials at 30 Ry for PW91. The simulations were carried out with the D mass instead of H, both for technical reasons[43] and in order to minimize quantum effects when comparing to experiments, together with a fictitious electron mass of $\mu = 800$ a.u. and a 5 a.u. time step. Each individual system was carefully equilibrated separately at 300 K followed by 20–50 ps of microcanonical dynamics. As a known reference, $H^+(aq)$ is investigated as well using the same

functionals and setups. This is done not only to compare computed time scales directly to time–resolved experiments,[20] but also to provide an internally consistent reference for the corresponding OH^-(aq) systems. In total, generating about half a nanosecond of AIMD trajectories was necessary in order to allow for such a systematic study of defect population correlation functions including comprehensive kinetic analyses.

Concerning systematic errors there is the issue of finite-size effects since the solvation-shells could couple to their periodic images. This has been investigated by doubling the system size from $N=31$ to 63 water molecules. Second, some recent literature including Ref. 52 brought up the issue of possible dynamical artifacts due to using finite μ in the Car–Parrinello dynamics (see the monograph[43] for a comprehensive discussion of this issue). In order to confirm our standard setup using $\mu=800$ a.u. together with the deuterium mass, this parameter has been decreased to $\mu=400$ a.u. together with a reduced time step of 3 a.u. Upon improving both parameters by a factor of 2 for the most important case, i.e., OH^-(aq) using BLYP, it can be seen from Table IV (see Sec. IV B) that there is neither a statistically significant effect due to N nor due to μ on the computed kinetics based on the qualitative scenarios extracted.

IV. RESULTS AND DISCUSSION

A. Positive charge defects: Checking time scales for H^+(aq)

From the previous discussion of the H^+(aq) mechanism, only one essential threefold solvation pattern for H_3O^+ exists even when distorted into the Zundel cation form. Based on this observation, if we assume simple first-order kinetics, the intermittent PT correlation functions $C_i(t)$ and $C_{nn}(t)$ should have the biexponential forms of Eqs. (14) and (18). Furthermore, from the integral equation theory of Sec. II B, the continuous PT correlation function $C_c(t)$ is also expected to feature such a biexponential decay.

In the Appendix, we will describe a fractional kinetic model for describing the long-time behavior of the correlations functions. However, we restrict our attention here to the biexponential form beause the AIMD simulations have not been carried out to sufficiently long time scales to see significant deviation from the biexponential form. Such deviations occur on the 50 ps time scale and would require at least 0.5 ns–1.0 ns to capture accurately. For example, the continuous PT correlation functions, $C_c(t)$, which are shown in Fig. 3(a), are assumed to fit the following three-parameter form:

$$C_c(t) = a_{fast} \exp[-t/\tau_1] + a_{slow} \exp[-t/\tau_2], \quad (44)$$

with $a_{fast}+a_{slow}=1$, on time scales of the order of $\sim$10 ps. The quality of a typical biexponential fit is shown in Fig. 4. The correlation coefficient for the fit is $\chi \geq 0.99$. Including the rattling events, two time scales, $\tau_1 \approx 30-50$ fs and $\tau_2 \approx 260$ fs, are found for both BLYP and HCTH (see Table I). They can be assigned to proton rattling in Zundel- and Eigen-like complexes, respectively. The difference between τ_1 and τ_2 results from the location of the proton relative to the instantaneous HB-midpoint: In Eigen-like complexes, larger amplitude vibrations and thus longer time scales are needed for the proton to return. The integrated, average lifetime of the positive charge defect is $\tau_{exch} \approx 200$ fs in both cases. For PW91, only one (intermediate) time scale of $\tau_2 \approx 100$ fs could be resolved (i.e., $a_{fast} \approx 0$). An independent view to this approach is given by extracting the PT rates from the short-time analysis of Eq. (14), which yields $1/k_1^{PT} \approx 80-220$ fs for the short-time dynamics. Considering all computed time scales, it can be concluded that proton

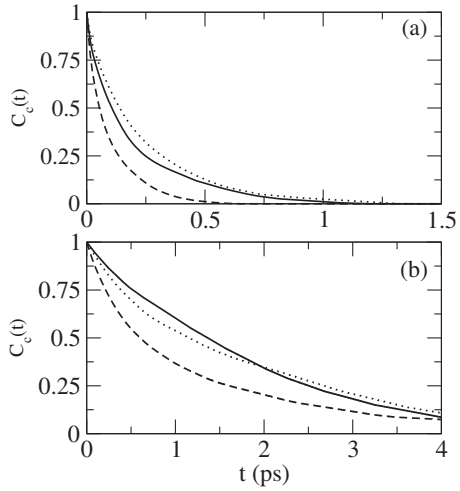

FIG. 3. Continuous correlation function, $C_c(t)$, of H^+(aq) obtained by using PW91 (dashed), BLYP (solid), and HCTH (dotted) functionals. (a) Rattling effects are included. (b) Rattling effects are excluded in the calculations of the correlation function.

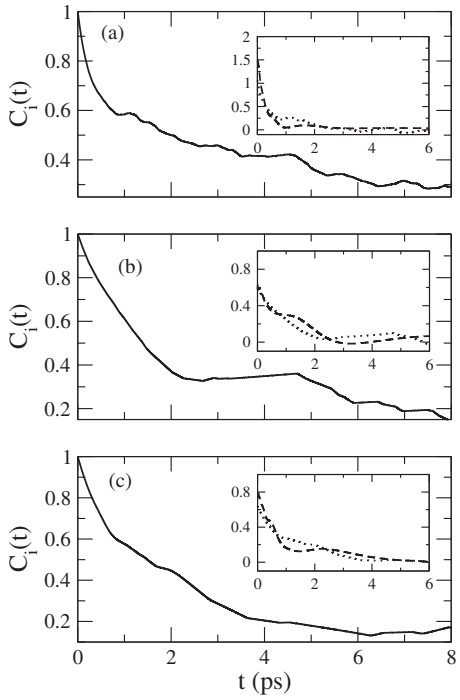

FIG. 4. Intermittent correlation function, $C_i(t)$, of H^+(aq) obtained by using (a) PW91, (b) BLYP, and (c) HCTH functionals. Rattling effects are excluded in the calculations of the correlation function. In the inset of each figure, dashed curve shows the results of $-dC_i/dt$ and dotted curve shows its fit to the rate expression as given by the right hand side of Eqs. (8) and (10). The corresponding rate constants are included in Table I.

TABLE I. Relaxation times and inverse rates (all in ps) for H^+(aq) including and excluding rattling events as defined in the text.

Functional	Rattling	τ_{exch}	$1/k_1^{PT}$	τ_1	τ_2	a_{slow}	$1/k_1^{HB\text{-}O_w}$
PW91	Included	0.10	0.08	⋯	0.10	1.00	2.15
	Excluded	1.24	1.00	0.36	1.85	0.60	2.15
BLYP	Included	0.19	0.14	0.05	0.26	0.66	2.20
	Excluded	1.66	1.68	⋯	1.75	1.00	2.20
HCTH	Included	0.23	0.22	0.03	0.26	0.85	1.40
	Excluded	1.70	1.57	0.15	1.88	0.93	1.40

rattling along HBs, which interchanges Eigen- and Zundel-like defects without net charge displacement, occurs on time scales roughly in the range of 50–200 fs independent of the particular model. Recall that no quantum effects on nuclear motion are included when computing these numbers. These are expected to facilitate proton rattling by flattening out the free energy profile along the PT coordinate.[9,56] Thus, the extracted time scale is consistent with the very short time scale of <100 fs ascribed to the interconversion of Eigen and Zundel complexes in femtosecond vibrational spectroscopy[20] and with recent AIMD calculations of the hydrated proton carried out with a converged real-space basis set.[61]

Consider, next, excluding the proton rattling events since they do not contribute to net charge displacement or proton transport. The decay of the continuous and intermittent PT correlations excluding proton rattling effects are shown in Figs. 3(b) and 4, respectively. Figure 5 shows the quality of fits of the continuous and intermittent correlation functions to the bi-exponential form in Eq. (44). For BLYP and HCTH the average charge defect lifetime is $\tau_{exch} \approx 1.7$ ps in both cases, which again is consistent with the corresponding inverse PT rates $1/k_1^{PT} \approx 1.6-1.7$ ps for true proton migration

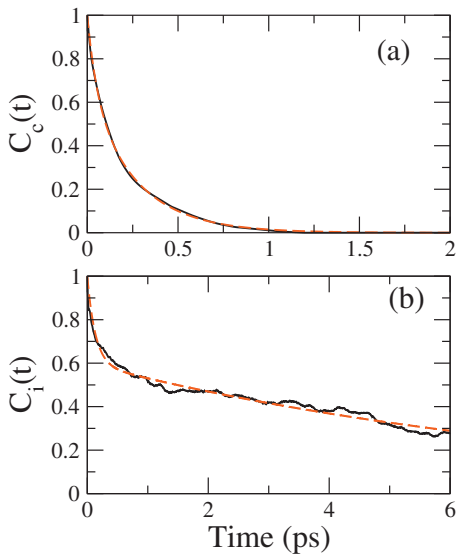

FIG. 5. (a) Continuous correlation function, $C_c(t)$, of H^+(aq) obtained by using BLYP (solid) and the fit of the correlation function to the biexponential form in Eq. (44) (red dashed). (b) Same for the intermitting correlation function $C_i(t)$. In both panels, rattling events are included.

(see Table I). At first sight, the corresponding process appears to be significantly faster for PW91 where $1/k_1^{PT} \approx \tau_{exch} \approx 1.0-1.2$ ps. However, there is still some contamination due to an underlying fast process that emerges only when $C_c^{OO}(t)$ is decomposed. For PW91, the slow process accounts for about $a_{slow} \approx 60\%$ of the overall decay, and for this process $\tau_2 \approx 1.85$ ps, which corresponds closely to 1.75 and 1.88 ps for BLYP and HCTH, respectively.

This demonstrates that those PT events that lead to structural diffusion of the defect occur on time scales of about 1–2 ps for all three functionals. This is of the same order as the HB fluctuations, but an order of magnitude slower than the aforementioned proton rattling time. HB dynamics is quantified by the lifetimes of HBs in bulk water, $1/k_1^{HB\text{-}O_w}$, and has been obtained by the well-established procedure,[33–35] from separate pure bulk water simulations. These bulk lifetimes (see Table I), i.e., 2.15, 2.20, and 1.40 ps for PW91, BLYP, and HCTH, respectively, are indeed close to the above computed time scale of structural diffusion; an estimate of about 2 ps is in fair agreement with the experimental HB lifetime[73] of ≈1.4 ps considering that quantum dynamics would speed up this process. Finally, it is noted that the experimental numbers are 1.7 or 1.3 ps (depending on the experimental probe) for structural diffusion events and of the order of 1 ps for solvent reorganization.[20]

In conclusion, the presented kinetics analysis of the three popular density functionals PW91, BLYP, and HCTH belonging to vastly different "families" of density functionals all yield a very similar and thus consistent quantitative picture for proton rattling, HB relaxation, and structural diffusion of H^+(aq) which is furthermore in accord with the pertinent experimental time scales.

B. Negative charge defects: Predicting time scales for OH^-(aq)

Turning next to the intriguing OH^-(aq) problem, there are now $p=2$ dominant solvation structures in which OH^- accepts either four or three HBs at its oxygen site denoted here by n_j=OO-4 and OO-3, respectively. This leads to two continuous PT correlation functions $C_c^{OO\text{-}4}(t)$ and $C_c^{OO\text{-}3}(t)$ according to the definition based on Eq. (22) and to corresponding lifetimes $\tau_{exch}^{OO\text{-}4}$ and $\tau_{exch}^{OO\text{-}3}$, depending on the particular solvation topology, according to Eq. (23). Furthermore, the chemical master equation now assumes the form in Eq.

TABLE II. Relaxation times and inverse rates (all in ps) for OH^-(aq) excluding rattling events as defined in the text. The HB lifetime for bulk water, $1/k_1^{\text{HB-O}_w}$, is given in parentheses following the $1/k_1^{\text{HB-O}^*}$ data.

Functional	τ_{exch} $1/k_1^{\text{PT}}$	$\tau_{\text{exch}}^{\text{OO-3}}$ $\tau_{\text{exch}}^{\text{OO-4}}$	$\tau_{\text{fast-1}}$ $\tau_{\text{fast-2}}$	$a_{\text{fast-1}}$ $a_{\text{fast-2}}$	τ_{slow} $1/k_1^{\text{HB-O}^*}$	$\tau_{\text{fast}}^{\text{mm}}$ $1/k_{-1}^{\text{HB-H}'}$
PW91	1.16	0.52	0.11	0.14	2.6	0.11
	0.74	2.50	0.66	0.52	1.9 (2.15)	0.50
BLYP	3.20	0.65	⋯	0.00	4.0	0.13
	3.20	3.95	0.40	0.06	5.6 (2.20)	0.30
HCTH	15.6	⋯	⋯	0.00	15.0	0.15
	13.8	15.6	⋯	0.00	14.0 (1.40)	0.30

(26), and the intermittent and continuous correlation functions are predicted to decay as triexponentials as in Eq. (28).

The average PT rates k_1^{PT} extracted from Eq. (26) *differ considerably* for the three functionals (see Table II), in stark contrast to the H^+(aq) case. Proton rattling is excluded at this stage of the analysis since we wish to focus first on structural diffusion and thus avoid further complications. The decay profiles of the continuous and intermittent correlations without rattling contributions are shown in Figs. 6 and 7, respectively. Consistent with the qualitative mechanistic picture discussed above, PW91 and HCTH predict maximal and minimal rates, respectively, whereas BLYP yields a rate in between these two limits. For PW91, the decay behavior of the continuous correlation function $C_c^{\text{OO}}(t)$ exhibits one slow and two fast relaxation times, τ_{slow}, $\tau_{\text{fast-1}}$, $\tau_{\text{fast-2}}$, with corresponding weights $a_{\text{slow}}+a_{\text{fast-1}}+a_{\text{fast-2}}=1$. For PW91 and BLYP, both fast and slow processes are found with relaxation times in the range of $\tau_{\text{fast}}\approx 0.5$ ps and $\tau_{\text{slow}}=3-4$ ps, amounting to essentially one order of magnitude difference between the two processes. The crucial difference is, however, the weights: the *fast processes* are *negligible* for BLYP, $a_{\text{fast-1}}+a_{\text{fast-2}}\approx 0.06$, whereas they are *dominant* for PW91, $a_{\text{fast-1}}+a_{\text{fast-2}}\approx 0.66$. Perhaps surprisingly, for HCTH there is *no fast process* at all, i.e., $a_{\text{fast-1}}+a_{\text{fast-2}}\approx 0$, within statistical accuracy, but $\tau_{\text{slow}}\approx 16$ ps corresponds to a *significantly slower* relaxation. Because one of the fast time scales for the BLYP case has zero weight, we can fit the continuous and intermittent correlation functions with a biexponential form. We demonstrate the quality of such a fit in Figs. 8(a) and 8(b), respectively, for $C_c(t)$ and $C_i(t)$. In these fits, rattling events are included. The figure shows that on the time scale captured by the AIMD simulations, the biexponential fit closely matches the data.

Having found these dramatic differences, the next step is to elucidate the underlying physical phenomena connected to these numbers. Guided by the interplay of solvation and

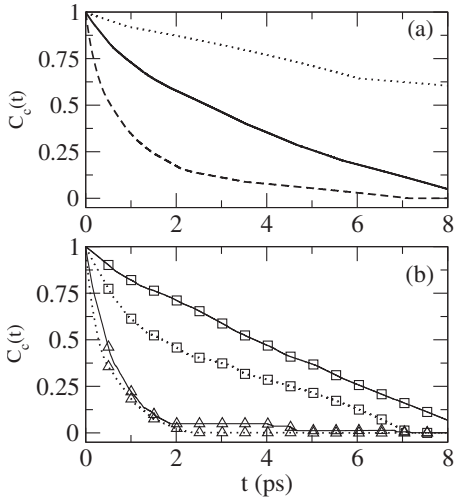

FIG. 6. (a) Continuous correlation function, C_c^{OO}, of OH^-(aq) obtained from PW91 (dashed), BLYP (solid), and HCTH (dotted) corresponding to mirror image, dynamical hypercoordination, and static hypercoordination mechanisms, respectively. (b) Continuous correlation functions of OH^-(aq) for O^* accepting exactly three (triangles), $C_c^{\text{OO-3}}$, or four (squares), $C_c^{\text{OO-4}}$, hydrogen bonds at the time origin $t=0$ obtained from PW91 (dashed) and BLYP (solid); $C_c^{\text{OO-3}}$ could not be determined for HCTH due to insufficient statistics (see also text and Table II). Rattling contributions are excluded in these calculations.

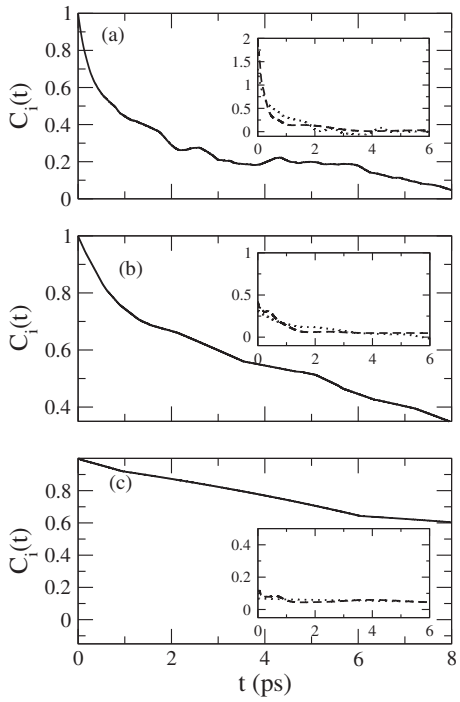

FIG. 7. Intermittent correlation function, $C_i(t)$, of OH^-(aq) obtained by using (a) PW91, (b) BLYP, and (c) HCTH functionals. Rattling effects are excluded in the calculations of the correlation function. In the inset of each figure, the dashed curve shows the results of $-dC_i/dt$ and the dotted curve shows its fit to the rate expression as given by the right hand side of Eq. (8). The corresponding rate constants are included in Table II.

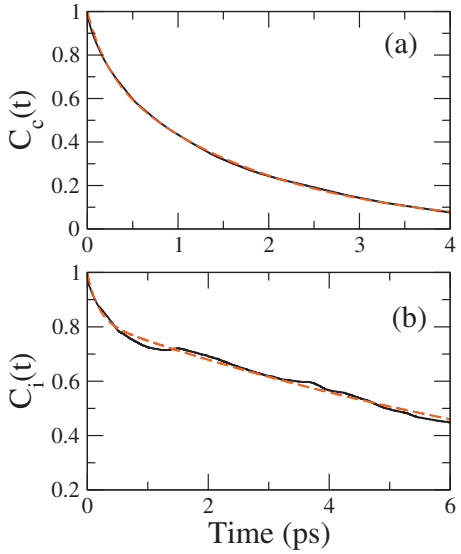

FIG. 8. (a) Continuous correlation function, $C_c(t)$, of OH^-(aq) obtained by using BLYP (solid) and the fit of the correlation function to a triexponential form (red dashed). (b) Same for the intermitting correlation function $C_i(t)$. In both panels, rattling events are included.

mechanism, the impact of the specific solvation pattern must be worked out. In order to do this, we make use of the solvation-topology-specific continuous correlation functions $C_c^{OO}(t)$ defined separately for those OH^-(aq) in which O^* accepts exactly either three or four HBs, i.e., $C_c^{OO\text{-}3}$ and $C_c^{OO\text{-}4}$, respectively. These are, then, used to compute exchange times $\tau_{exch}^{OO\text{-}4}$ and $\tau_{exch}^{OO\text{-}3}$ using Eq. (23). Comparing both $\tau_{exch}^{OO\text{-}4}$ and $\tau_{exch}^{OO\text{-}3}$ to the fast and slow processes (i.e., to $\tau_{fast\text{-}1}$, $\tau_{fast\text{-}2}$, and τ_{slow}), the *slow process* is consistently found to be associated with PT from *fourfold coordinated* OH^-(aq) since $\tau_{slow} \approx \tau_{exch}^{OO\text{-}4}$ *for all three functionals* (see Table II). On the other hand, it is $\tau_{exch}^{OO\text{-}3}$ and thus the *threefold coordinated* OH^-(aq) species that can be linked exclusively to the fast processes, $\tau_{fast\text{-}1}$ and $\tau_{fast\text{-}2}$. Most importantly however, the relations

$$\tau_{fast} \approx \tau_{exch}^{OO\text{-}3} \ll \tau_{exch}^{OO\text{-}4} \approx \tau_{slow}$$

strongly support our mechanistic picture as formulated based on the presolvation concept: PT occurs preferentially if the proton-receiving species is properly solvated—a concept that holds *independently* of the functional and its predicted mechanism.

The next task is to connect these vastly different time scales to elementary processes in the liquid. Guided by the success of the H^+(aq) analysis, the first candidate is the HB lifetime in the bulk. However, the negligible differences reported earlier for $1/k_1^{HB\text{-}O_w}$ using PW91, BLYP, and HCTH (see Table I) cannot explain the vastly different structural diffusion behavior of OH^-(aq). Next, the lifetimes of HBs existing (at time $t=0$) between the defect site, O^*, and first shell solvation water only, $1/k_1^{HB\text{-}O^*}$, were computed. Here, the three time scales all turn out to be close to each other,

$$1/k_1^{HB\text{-}O^*} \approx \tau_{slow} \approx \tau_{exch}^{OO\text{-}4},$$

for all three functionals (see Table II). This is consistent with the idea that fluctuations of HBs between OH^- and water molecules in its first shell drive structural diffusion for both BLYP and HCTH. For HCTH, however, this HB lifetime is unusually long, $1/k_1^{HB\text{-}O^*} \gg 1/k_1^{HB\text{-}O_w}$, implying that the first shell is very tightly bound to OH^- thus supporting the existence of rather long-lived solvation-shell aggregates, $[OH^- \bullet (H_2O)_n](aq)$, and thus a dominant contribution of hydrodynamic vehicle diffusion. Although both BLYP and HCTH feature hypercoordination, the first solvation-shell around the defect O^* is a dynamical object according to BLYP, whereas it is rigid for HCTH.

For PW91, in stark contrast, the two HB lifetimes exceed by far, and thus do not match the fast relaxation times, i.e.,

$$1/k_1^{HB\text{-}O_w} \approx 1/k_1^{HB\text{-}O^*} \gg \tau_{fast\text{-}1}, \quad \tau_{fast\text{-}2}.$$

On the other hand, it has already been shown that the fast relaxation times are the dominant contributions to PT for PW91 in view of $a_{fast\text{-}1}+a_{fast\text{-}2}$ amounting to about 70%. This implies that other microscopic processes must correlate with the PT rate for PW91. A much faster process than HB breaking and making is the ultrafast reorientational motion in the solvation-shell of OH^- as probed by the *short-time* decay of the following orientational correlation function:

$$C^{mm}(t) = \frac{\langle \mathbf{m}(t) \cdot \mathbf{m}(0) \rangle}{\langle \mathbf{m}^2 \rangle}. \tag{45}$$

Here, $\mathbf{m}(t)$ is the purely geometric dipole vector of a H_2O molecule at time t and the average includes only H_2O molecules in the first hydration shell of OH^-(aq) at time $t=0$ and the corresponding exponential decay time is denoted τ_{fast}^{mm}.

The reorientational time scale τ_{fast}^{mm} obtained is essentially identical for all three cases (see Table II), but the crucial observation is that it matches only the ultrafast component of the PT rate for PW91, $\tau_{fast\text{-}1}$. Furthermore, the rate constant for HB formation involving the hydrogen H′ of OH^-(aq), $k_{-1}^{HB-H'}$, that is the donated HB, is computed. Its inverse is found to match $\tau_{fast\text{-}2}$ for PW91 and BLYP in Table II; note that HCTH only features a slow channel to PT, τ_{slow}. Thus, if the *donated* HB is formed by OH^-(aq) through the OH^- hydrogen, H′, then PT is triggered by ultrafast rotational/reorientational motion of surrounding water molecules; otherwise this $H'\cdots O_w$ HB needs to be formed first for proper presolvation before PT can occur. In conclusion, this analysis naturally explains, at the level of molecular kinetics, "…why the simulation rates are higher than observed experimental rates" (quoted from Ref. 52) for OH^-(aq) when using the PW91 functional.

The full picture is obtained upon quantifying proton rattling as well. In Fig. 9, we have shown the time dependence of the continuous correlations of OH^-(aq) when proton rattling events are included. Results are also shown for the decay of $C_c(t)$ when OH^- accepts three and four HBs at time $t=0$. The data in Table III show that the associated time scale is, for all functionals, considerably faster when OH^- accepts three HBs in comparison with the fourfold coordinated state since $\tau_{exch}^{OO\text{-}4} \gg \tau_{exch}^{OO\text{-}3}$ always holds. Recall that rattling cannot be detected for HCTH within the available statistics since OH^- is rarely found in the threefold solvated state. Comple-

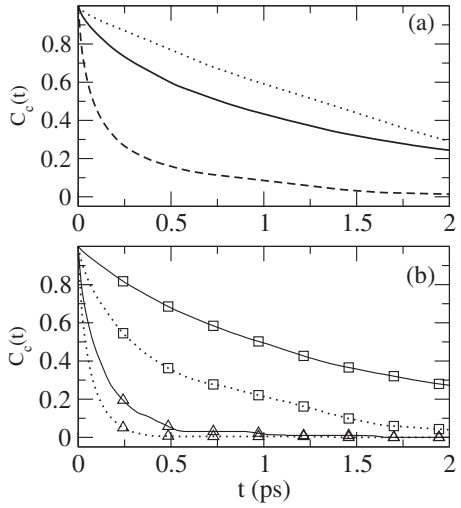

FIG. 9. (a) Continuous correlation function, $C_c(t)$, of OH^-(aq) obtained by using PW91 (dashed), BLYP (solid), and HCTH (dotted) functionals. Rattling effects are included in the calculations of the correlation function. (b) Continuous correlation functions of OH^-(aq) for O^* accepting exactly three (triangles), C_c^{OO-3}, or four (squares), C_c^{OO-4}, hydrogen bonds at the time origin $t=0$ obtained from PW91 (dashed) and BLYP (solid). Again, rattling effects are included in these calculations.

mentary to this decomposition in terms of solvation-shell patterns is the decay analysis of $C_c^{OO}(t)$ in the time-domain. A biexponential fit is found to describe all cases satisfactorily, and including a third channel does not yield a distinct third relaxation time. Interestingly, it is found that the slow time scale τ_{slow}, for all functionals, closely matches the time τ_{exch}^{OO-4} that fourfold coordinated complexes spend on average without any PT, be it rattling or real PT contributing to charge defect migration (i.e., PW91: 0.60 versus 0.54, BLYP: 1.70 versus 1.55, HCTH: 1.76 versus 1.80). Most important, however, is the observation that for PW91 only, the two time scales τ_{fast} and τ_{slow} (i.e., 0.06 and 0.60) are essentially identical to τ_{fast-1} and τ_{fast-2} (i.e., 0.11 and 0.66) found for real PT and thus structural diffusion according to Table II. This crucial finding implies that for PW91 *only*, rattling and structural diffusion must occur on the *same* time scale!

Having analyzed the time scales obtained within the standard setup, the impact of systematic errors due to using finite particle number N and finite fictitious electron mass μ must be investigated. This is done by doubling N and by decreasing μ to half its standard value for the most important

TABLE III. Relaxation times and inverse rates (all in ps) for OH^-(aq) including rattling events as defined in the text.

Functional	τ_{exch} $1/k_1^{PT}$	τ_{exch}^{OO-3} τ_{exch}^{OO-4}	τ_{fast} a_{fast}	τ_{slow} a_{slow}
PW91	0.27	0.08	0.06	0.60
	0.09	0.54	0.61	0.39
BLYP	1.35	0.16	0.18	1.70
	0.59	1.55	0.20	0.80
HCTH	1.78	⋯	⋯	1.76
	1.65	1.80	0.00	1.00

scenario, i.e., the dynamical hypercoordination mechanism predicted by BLYP. Assessing these error bounds, the threefold coordinated species feature proton rattling on an average time scale in the range of $\tau_{exch}^{OO-3} \approx 160-310$ fs, which compares well with the fast decay component $\tau_{fast} \approx 120-350$ fs of $C_c^{OO}(t)$ (see Table IV). In the fourfold solvated complex, on the other hand, OH^-(aq) lives on average for about $\tau_{slow} \approx 1.7-2.1$ ps without *any* PT event in between, which correlates well with the time scale of structural diffusion. Furthermore, the short and long-time scales for relaxation of threefold complexes are $\tau_{fast}^{OO-3} \approx 30-70$ fs and $\tau_{slow}^{OO-3} \approx 220-450$ fs, respectively, whereas these time scales are $\tau_{fast}^{OO-4} \approx 340-420$ fs and $\tau_{slow}^{OO-4} \approx 1.8-2.4$ ps, respectively, for the fourfold solvation pattern when considering these errors as obtained from the biexponential analysis of C_c^{OO-3} and C_c^{OO-4}, respectively. Clearly, the slower component of the threefold species is, within the error interval, identical to the faster component of the lifetime of the complexes that accept four HBs. Thus, the numbers are found to change, but their relative order, which is relevant for the mechanistic scenario, is not affected.

The extremely short lifetime of about $\tau_{fast}^{OO-3} \approx 50 \pm 20$ fs is quite distinct and is known to result from a very efficient decay of those transiently created OH^-(aq) defects that are properly presolvated for PT once they accept three HBs. There is hope that time-resolved experiments of the sort pioneered previously for H^+(aq) systems[17–21,23,25] together with the use of more dilute solutions will provide clues by which the time scale of approximately 160 fs that has been detected in a quite concentrated 10*M* solution of NaOD in D_2O previously[74] can be disentangled; note that this concentration corresponds to a ratio of hydroxide anions to water molecules of about 1:5.2, which is known to decrease the coordination number of the OH^- solvation-shell compared to more dilute references.[50,75,76] The aforementioned 160 fs time scale has been tentatively assigned to deuteron hopping[74] whereas a different explanation in terms of overtone transitions due to transient $H_3O_2^-$ species is offered in Ref. 77. Indeed, the observed time scale of 110 fs assigned to such short-lived complexes has been attributed in Ref. 77 to the time scale of PT including proton rattling events as predicted in Table II of Ref. 16, i.e., to $\tau_{fast} \approx 180$ fs or $\tau_{exch}^{OO-3} \approx 160$ fs as provided in Table III herein. Based on the present assessment of systematic errors (see Table IV), one must consider error intervals of $\tau_{fast} \approx 120-350$ fs and $\tau_{exch}^{OO-3} \approx 160-310$ fs for these time scales, and one must remember that the experimental time scales are expected to be shorter because these AIMD simulations are fully deuterated while the experiments are not. Nevertheless, detecting the fastest time scale possible, i.e., $\tau_{fast}^{OO-3} \approx 50 \pm 20$ fs arising from those OH^-(aq) defects that accept three HBs as the presolvated precursor to PT remains a challenge for future ultrafast experiments.

In addition to processes due to translational diffusion of O^*, the molecular axis of OH^- is expected to undergo an interesting rotational dynamics and thus rotational relaxation accessible to recent experiments. The rotational motion of a molecule in bulk solution can be measured via the rotational anisotropy function $r(t)=(S_\parallel - S_\perp)/(S_\parallel + 2S_\perp)$, where $S_\perp$ and

TABLE IV. Relaxation times and inverse rates (all in ps) for OH^-(aq) including rattling events obtained with the BLYP functional comparing a larger system size N and a smaller fictitious electron mass μ to the standard settings (N=31 water molecules and μ=800 a.u.) reported in the first row. The weights a_i according to biexponential fits are given in parentheses; see text for details.

BLYP	τ_{exch} $1/k_1^{PT}$	$\tau_{exch}^{OO\text{-}3}$ $\tau_{exch}^{OO\text{-}4}$	τ_{fast} τ_{slow}	$\tau_{fast}^{OO\text{-}3}$ $\tau_{slow}^{OO\text{-}3}$	$\tau_{fast}^{OO\text{-}4}$ $\tau_{slow}^{OO\text{-}4}$
N=31, μ=800	1.35	0.16	0.18 (0.20)	0.05 (0.42)	0.40 (0.18)
	0.59	1.55	1.70 (0.80)	0.22 (0.58)	1.80 (0.82)
N=63, μ=800	1.70	0.27	0.35 (0.20)	0.03 (0.12)	0.42 (0.25)
	1.00	1.90	2.10 (0.80)	0.30 (0.88)	2.40 (0.75)
N=31, μ=400	1.64	0.31	0.12 (0.10)	0.07 (0.46)	0.34 (0.05)
	0.98	1.80	1.80 (0.90)	0.45 (0.54)	1.90 (0.95)

$S_\parallel$ are signals measured in directions perpendicular and parallel to the pump polarization. In the absence of couplings between molecular rotations and other degrees of freedom and for a long enough time delay between the pump and probe pulses, this rotational anisotropy function can be expressed in terms of a rotational correlation function[78]

$$r(t) = 0.4\langle P_2[\mathbf{u}(0)\cdot\mathbf{u}(t)]\rangle, \tag{46}$$

where $P_2(x)=(3x^2-1)/2$ is the Legendre polynomial of second order and $\mathbf{u}(t)$ is the unit vector along the molecular vector of interest. Thus, $\mathbf{u}(0)\cdot\mathbf{u}(t)=\cos\theta(t)$ defines the angle between this vector at times 0 and t, which is the O–H axis of the hydroxide ion in the following.

Recently, spectroscopic studies of the temporal decay of the rotational anisotropy of OH^- in water have been carried out[79,80] and yielded time constants of 1.9 ps (Ref. 80) and 3 ps (Ref. 79) for the long-time decay of $r(t)$ at room temperature. In addition, recent time-dependent vibrational spectroscopic studies have reported time scales of 2.6 ps (Refs. 81–83) and 3.0 ps (Ref. 84) for the long-time rotation of HOD in (pure) light and heavy water, respectively. Considering that the above long-time values carry a weight of about 80–85% (Refs. 81 and 83) and that the short-time inertial relaxation occurs very fast with a time scale in the range of 100 fs or less,[82] the above long-time results for liquid water are consistent with earlier NMR relaxation studies which reported a time scale of approximately 2 ps for the integrated relaxation time of rotational motion in light water.[85,86] Hence, for the *long-time* diffusive part of the dynamics, OH^- in water shows a *faster*[80] or comparable[79] rotational relaxation when compared to that of water molecules in the bulk.

A recent computational study of the reorientation of hydroxide in water[87] as a function of temperature showed good agreement with the experimental results of Ref. 79. In this study, the integrated relaxation time of the normalized correlation function akin to Eq. (46) was compared with the experimental results of Ref. 79. However, since the experimental time scales are deduced from the long-time decay of the rotational anisotropy, a more direct comparison should involve the calculated relaxation time for the long-time decay of $r(t)$ rather than its integrated time constant. Another important caveat of the study in Ref. 87 is the fact that it is based on an empirical force field model that does not allow for PT events. Because the latter lead to changes in the identity of O^*, and thus to reorientational jumps in view of the locally tetrahedral symmetry, it is likely that they contribute in a nontrivial way to the observed reorientation time, particularly at temperatures near and above room temperature. This is indeed confirmed by the present study as will be shown in the following paragraphs.

In order to compare the predicted scenarios of the three different density functionals employed in the present work to the experimental relaxation data,[79,80] the decay constants τ_r of the rotational anisotropy of OH^-(aq) have been obtained from Eq. (46) as summarized in Table V. In addition to calculating the rotational relaxation time of hydroxide ion in water, we have obtained the corresponding rotational relaxation time of the water molecules from analogous pure water simulations. Since the calculated decay of $r(t)$ includes both

TABLE V. Rotational relaxation times (weights) of OH^-(aq) and bulk water molecules (all given in ps); note that the deuterium mass is used for H throughout. The rotational relaxation times of water molecules in the bulk are obtained from separate pure bulk water simulations. The experimental values of hydroxide and water rotational relaxation correspond to those of (a) OH^- (Ref. 80), (b) OH^- (Ref. 79), and (c) HOD in light water (Refs. 81–83), respectively. Note that $a_{r\text{-}fast}+a_{r\text{-}slow}=0.4$ in order to satisfy Eq. (46).

Quantity	PW91	BLYP	HCTH	Experiment
$\tau_{r\text{-}fast}^{OH^-}$ ($a_{r\text{-}fast}^{OH^-}$)	0.18 (0.24)	0.12 (0.12)	0.05 (0.07)	
$\tau_{r\text{-}slow}^{OH^-}$ ($a_{r\text{-}slow}^{OH^-}$)	3.05 (0.16)	6.7 (0.28)	17.5 (0.33)	1.9(a), 3.0(b)
$\tau_{r\text{-}fast}^{H_2O}$ ($a_{r\text{-}fast}^{H_2O}$)	0.08 (0.08)	0.10 (0.10)	0.11 (0.10)	
$\tau_{r\text{-}slow}^{H_2O}$ ($a_{r\text{-}slow}^{H_2O}$)	17.5 (0.32)	11.5 (0.30)	5.75 (0.30)	2.6(c)
$\tau_{r\text{-}slow}^{OH^-}/\tau_{r\text{-}slow}^{H_2O}$	0.17	0.58	3.04	0.73(a),(c), 1.15(b),(c)

short-time inertial and long-time diffusive relaxation, the entire decay has been fit to a biexponential function of the form

$$r(t) = a_{\text{r-fast}} \exp[-t/\tau_{\text{r-fast}}] + a_{\text{r-slow}} \exp[-t/\tau_{\text{r-slow}}], \quad (47)$$

such that $a_{\text{r-fast}}+a_{\text{r-slow}}=0.4$ thus satisfying Eq. (46). The calculated relaxation times and associated weights are collected in Table V where they are also compared to the available experimental results. Note that the theoretical results of OH^- rotation are obtained by excluding the rattling effects. In fact, as in the case of translational diffusion, inclusion of such rattling effects only alters the short-time part of the rotational dynamics, while the long-time diffusive part of the dynamics, which is the main focus here, remains essentially unaltered. It should also be noted that the rotational times computed for pure bulk water are in accord with those reported earlier for the same functional.[88]

As in the case of translational diffusion[7] the more meaningful quantity to compare to experiment is the *ratio* of the rotational constants of OH^- and H_2O, i.e., $\tau^{OH^-}_{\text{r-slow}}/\tau^{H_2O}_{\text{r-slow}}$, as given in the last row of Table V. It is clear from this table that only the scenario obtained from BLYP provides a ratio for the rotational relaxation times that is meaningful when compared to experiments. This is in stark contrast to PW91 which predicts a significantly smaller value for this ratio whereas, not unexpectedly, the HCTH functional leads to a value that is clearly too large. In conclusion, rotational motion of OH^- in water is much too fast using PW91, and too slow in the HCTH scenario, which is consistent with the findings from the kinetics analyses.

We note that the orientation of OH^-(aq) was believed to be little affected by proton transfer in Ref. 87. However, it is clear from the present results of BLYP and HCTH that structural diffusion allows OH^-(aq) to rotate much more efficiently compared to simple molecular anions in water. This is because the orientation of the O–H axis necessarily changes significantly and abruptly during each PT event as a result of charge migration. Since few orientational changes are expected to occur when OH^-(aq) stays as a hypercoordinated species, while major reorientation does take place during structural diffusion, it is expected that the slower diffusive component of the reorientational time of OH^- would roughly correspond to the lifetime of the hydrated OH^-(aq) in its resting state, i.e., the time spent when OH^- accepts four HBs in a roughly square-planar arrangement before it undergoes PT. This is indeed found to be the case for all three scenarios investigated where the relation

$$\tau^{OH^-}_{\text{r-slow}} \approx \tau_{\text{slow}} \approx \tau^{\text{OO-4}}_{\text{exch}}$$

holds to a significant extent according to Tables V and II. This underlines the internal consistency of these vastly different analyses of the dynamics; however, one must keep in mind that the lifetime $\tau^{\text{OO-4}}_{\text{exch}}$ of this resting state, being inactive with respect to PT, is much too short using PW91 and too long in the HCTH scenario.

Last but not least, the effects of finite system size N and finite fictitious electronic mass μ on the rotational relaxation times of OH^-(aq) are investigated for the dynamical hypercoordination mechanism obtained for BLYP as done before for the kinetics analyses (see Table VI). Since separate pure bulk water simulations are only available for the so-called standard setup, the rotational relaxation times of water molecules have been obtained from those molecules which are outside the solvation-shell of OH^- in the simulations that include the hydroxide ion defect. This is a good approximation in view of the fact that these values are close to those obtained from separate pure bulk water simulations within the standard setup, i.e., $\tau^{H_2O\text{-same}}_{\text{r-fast}}=0.14$ ps $\approx \tau^{H_2O}_{\text{r-fast}}=0.10$ ps and $\tau^{H_2O\text{-same}}_{\text{r-slow}}=9.8$ ps $\approx \tau^{H_2O}_{\text{r-slow}}=11.5$ ps according to Tables VI and V, respectively. As before, it is seen that the relaxation times and especially the ratios of the rotational relaxation times of hydroxide and water molecules change only insignificantly for the larger system or for the system with the smaller fictitious electronic mass, when compared to those obtained with the standard setup using $N=31$ and $\mu=800$ a.u. Thus, this analysis fully supports the main conclusions drawn above regarding the vastly different rotational relaxation time of OH^-(aq) relative to that of the water molecules according to the PW91, BLYP, and HCTH functionals yielding the mirror image, dynamical hypercoordination, and static hypercoordination mechanisms, respectively.

TABLE VI. Rotational relaxation times (weights) of OH^-(aq) and bulk water molecules (all given in ps) obtained with the BLYP functional comparing a larger system size N and a smaller fictitious electron mass μ to the standard parameter settings ($N=31$ water molecules and $\mu=800$ a.u.) reported in the second column. The $\tau_r^{H_2O\text{-same}}$ and $a_r^{H_2O\text{-same}}$ data are obtained from the dynamics of the tagged "non-solvation-shell water molecules" in the simulations that include the hydroxide ion defect. Note that $a_{\text{r-fast}}+a_{\text{r-slow}}=0.4$ in order to satisfy Eq. (46).

Quantity	$N=31/\mu=800$	$N=63$	$\mu=400$
$\tau^{OH^-}_{\text{r-fast}}$ ($a^{OH^-}_{\text{r-fast}}$)	0.12 (0.12)	0.05 (0.08)	0.04 (0.07)
$\tau^{OH^-}_{\text{r-slow}}$ ($a^{OH^-}_{\text{r-slow}}$)	6.7 (0.28)	3.80 (0.32)	5.72 (0.33)
$\tau^{H_2O\text{-same}}_{\text{r-fast}}$ ($a^{H_2O\text{-same}}_{\text{r-fast}}$)	0.14 (0.10)	0.10 (0.07)	0.10 (0.08)
$\tau^{H_2O\text{-same}}_{\text{r-slow}}$ ($a^{H_2O\text{-same}}_{\text{r-slow}}$)	9.8 (0.30)	10.9 (0.33)	10.1 (0.32)
$\tau^{OH^-}_{\text{r-slow}}/\tau^{H_2O\text{-same}}_{\text{r-slow}}$	0.68	0.35	0.57

C. Dynamical hypercoordination mechanism for OH^-(aq): Experimental confirmations

Based on a wealth of dynamic and kinetic parameters, we have seen in the previous analyses that three different density functionals yield three qualitatively different structural diffusion mechanisms for OH^-(aq), whereas they all yield a consistent mechanism for the closely related H^+(aq) system. The remaining core issue, obviously, is a comparison to experiment in order to decide if the dynamical hypercoordination (predicted by BLYP), the static hypercoordination (obtained from HCTH), or the mirror image (according to PW91) mechanism is consistent with measurements.[8]

Subsequent to the AIMD predictions[12–15,49] of hypercoordination of OH^-(aq) and the dynamical hypercoordination mechanism—at that time being "…in contradiction to traditional views in chemistry textbooks …" (quoted from Ref. 49)—a comprehensive series of neutron scattering experiments[75,76,89–91] was launched. This systematic investigation of OH^-(aq) solvation structures provided strong evidence for dynamical hypercoordination. In particular, the

data[89] obtained with an aqueous 4.6*M* NaOH solution were found to be compatible with the presence of hypercoordinated (though nonplanar) hydrogen-bonded complexes yielding a first peak at ≈2.3 Å in the oxygen-oxygen radial distribution function, compared to approximately 2.8 Å in the bulk. The coordination number of the hydroxide ion was found to be 3.9 ± 0.3 in Ref. 75. In addition to providing evidence for *four* accepted water molecules, the data[89] revealed the presence of a fifth water molecule that is weakly hydrogen-bonded to the hydroxyl hydrogen site at an oxygen-oxygen distance between 2.75 and 3.20 Å with respect to the OH^- ion. This leads to about *one* (1.0 ± 0.2) water molecule at a distance from the hydroxyl hydrogen site between 1.77 and 2.22 Å in addition to the four accepted ones.

The concentration dependence of the solvation-shell was subsequently investigated.[75] As expected, the solvation number decreases from 3.9 ± 0.3 tightly bound water molecules for 1:12 and 1:9 solute:solvent molecules to 3.5 ± 0.3 and 2.9 ± 0.3 when the solute concentration goes up to 1:6 or 1:3, respectively. The spatial distribution functions for water molecules around the hydroxide remain nearly invariant, thus suggesting that only the population of the hydration shell changes as a function of concentration, but *not* its structure.[75] Subsequently, the concentration of hydroxide was further decreased[76] using a 2*M* NaOH solution, corresponding to about one OH^- per 28 water molecules. This OH^-:water ratio is close to one OH^- per 31 water molecules, which is the standard setup used in AIMD simulations[7,12–16] subject to periodic boundary conditions, see Sec. III B. Again, a coordination number of about four strongly hydrogen-bonded water molecules is found as well as exactly one additional weakly bound water molecule beyond this tight shell.[76] Finally, the possible influence of different alkali counterions, in particular, Li^+, Na^+, and K^+, on the hypercoordination of OH^-(aq) was assessed systematically[90] using solute:solvent concentrations ranging from 1:3 down to 1:12. Varying the counterion does not affect the overall shape of either the radial or spatial distribution functions, thus confirming the earlier conclusions.[75,89] Most recently, an x-ray diffraction study[67] of aqueous NaOH solutions of varying concentration supports both hypercoordination of the hydroxide anion in basic solutions and also its ability to donate a HB via hydration of the hydroxyl hydrogen.

At this stage it can be concluded that both neutron and x-ray diffraction experiments[67,75,76,89–91] strongly support the picture that OH^-(aq) does indeed prefer to accept four HBs. In addition, the diffraction data give clear evidence for a fifth, weak bond donated by the OH^- hydrogen. Based on these investigations, the authors in Ref. 90 draw the following conclusion: "It is demonstrated that the symmetry argument between H^+ and OH^- (*i.e., the mirror image concept*) cannot be used, at least in the liquid phase at such high concentrations, for determining the hydroxide hydration shell." (quoted from Ref. 90).

Recent investigations using spectroscopy instead of diffraction yield complementary support of an OH^-(aq) solvation-shell that follows the pattern of dynamical hypercoordination. The Fourier transform infrared spectroscopy was employed to investigate selected alkali metal hydroxide solutions.[92,93] No evidence was found for the existence of a stable $H_3O_2^-$ complex in these basic solutions, which is consistent with such a transient solvation complex being short-lived according to the dynamical hypercoordination mechanism. The existence of a weak interaction with a single water molecule at the hydrogen site of OH^-, i.e., the donated HB by the hydroxyl hydrogen required in dynamical hypercoordination, was confirmed by the spectral data as well.[92] Furthermore, x-ray absorption spectroscopy of aqueous KOH solutions has been carried out at two concentrations.[94] Comparison between the experimental data and *ab initio* calculations suggest that hydroxide exists in a hypercoordinated solvation state with respect to the number of accepted HBs; however, it is clearly spelled out that unambiguous identification was not possible at that time.[94]

More recently, the interaction of the hydroxide anion with solvation-shell water was studied directly using core-level photoelectron emission spectroscopy in a jet of NaOH and KOH aqueous solution.[95] Using the phenomenon of "intermolecular Coulombic decay" (ICD) it could be shown that the hydrated hydroxide anion behaves distinctly different from simple anions, such as F^-(aq) and Cl^-(aq), in terms of solvation-shell structure. In particular, the ICD data show that OH^-(aq) is capable of *transiently donating* a HB to surrounding water molecules: "We conclude that the resonance spectral structure observed in this study must be a microscopic signature of the OH^-(aq) hydrogen-bond donor" (quoted from Ref. 95). Thus, in agreement with previous experiments on aqueous hydroxide solutions, the findings in Ref. 95 support the notion that the (dynamically hypercoordinated) hydration structure of OH^-(aq) cannot be inferred from that of the hydrated excess proton.[95] In particular, "a direct and model-independent consequence of this interpretation of the unique spectral features is that it calls for a OH^-(aq) hydration pattern similar to the one invoked[4,5] (*these references correspond to Refs.* 7 and 15 *herein*) in one of the two competing mechanisms (i.e., dynamical hypercoordination) put forward to explain the anomalously fast transport of OH^- in aqueous solution" (quoted from Ref. 95). "The alternative transport mechanism is based on the 'proton-hole' concept[2,21] (*these references correspond to Refs.* 48 and 52 *herein*), which treats the hydroxide ion as a water molecule with a missing proton and OH^- transport as the mirror image process of proton structural diffusion… Our findings are not in agreement with the predictions of the proton-hole concept" (quoted from Ref. 95). Finally "as noted above, a plethora of experimental data support the presence of different coexisting OH^- hydration structures in aqueous solution as demanded by the first of the OH^- transport mechanisms (i.e., dynamical hypercoordination) discussed" (quoted from Ref. 95).

Dynamical information about the occurrence of $H_3O_2^-$ species in bases, which is predicted to be a transient complex in the dynamical hypercoordination mechanism, comes from time-resolved and two-dimensional IR experiments of dilute HDO in aqueous solutions of NaOD dissolved in heavy water.[77] These experiments[77] provide detailed insights into the lifetime of the intermediate $H_3O_2^-$ complex,

$[HO\cdots H\cdots OH]^-$, in basic solution, which is the mirror image analog of the $H_5O_2^+$ (Zundel) complex, $[H_2O\cdots H\cdots OH_2]^+$, in acidic solution. In particular,[77] these "results show the fleeting existence of Zundel-like $H_3O_2^-$ states that arise in the course of structural diffusion of the hydroxide ion" (quoted from Ref. 77) and they furthermore "indicate that this state exists transiently for 2–3 vibrational periods during the transfer of the proton" (quoted from Ref. 77). The authors of Ref. 77 also state, in reference to our recent AIMD simulations,[16] that "these simulations found 2 principal time scales that contribute to the proton transfer rate, a fast time scale of 180 fs that corresponds to 'proton rattling' events in which the proton returns to the original oxygen atom after a series of PT events within a Zundel-like state, and a slower 1.7-ps process that acts to gate the formation of Zundel-like configurations (10) (*this reference corresponds to Ref.* 16 *in this review*). Given that the simulations use a fully deuterated bath, the time scale for proton rattling agrees well with our experimentally observed value of 110 fs" (quoted from Ref. 77). In summary, femtosecond pump-probe spectroscopy confirms the *transient existence* of the Zundel-analog complex, $H_3O_2^-$, which is also a distinct feature of the dynamical hypercoordination mechanism. By contrast, according to the mirror image mechanism, the $H_3O_2^-$ complex is predicted to be a stable state and thus a longer-lived solvation structure of OH^-(aq), in close analogy to the $H_5O_2^+$ complex in the H^+(aq) system.

Results from electrochemistry shed additional light on the experimental picture. It is established[53] by conductivity measurements that the diffusion coefficient of H^+(aq) is significantly larger than that of OH^-(aq): 9.31 versus 5.30×10^{-9} m^2/s, respectively; note that the OH^-(aq) diffusion coefficient reported in Table II2.8 of Ref. 53 is misprinted as 5.03×10^{-9} m^2/s. Both diffusion coefficients are anomalously large since they exceed, by far, those of typical simple ions in ambient water,[53] for instance, 1.33 and 2.03×10^{-9} m^2/s for Na^+(aq) and Cl^-(aq), respectively, which are known to migrate hydrodynamically via the vehicular diffusion mechanism. Recalling that the self-diffusion coefficient of water is 2.26×10^{-9} m^2/s, it is evident that diffusion of OH^-(aq) is significantly faster than water self-diffusion but also much slower than H^+(aq) migration, i.e.,

$$D_{H^+} \gg D_{OH^-} \gg D_{H_2O},$$

holds in the sense of a robust, qualitative relationship. Thus, as advocated in Ref. 7, comparing diffusion coefficient ratios to experimental data should provide a robust test for scrutinizing simulated mechanistic scenarios *qualitatively*, irrespective of quantitative deviations. Referring to data reported in Ref. 7 we only mention here that structural diffusion of OH^-(aq) according to the mirror image mechanism as obtained from PW91 is unacceptably fast, $D_{H^+} \ll D_{OH^-}$, and exceeds even that of H^+(aq), which is the fastest case known.[53] For HCTH, the OH^-(aq) diffusion coefficient in the static hypercoordination scenario is similar to the self-diffusion coefficient of bulk water, $D_{OH^-} \approx D_{H_2O}$, which is much too slow in the static hypercoordination picture. The dynamical hypercoordination mechanism provided by BLYP predicts that OH^-(aq) is both considerably slower than H^+(aq) and faster than water self-diffusion, $D_{H^+} \gg D_{OH^-} \gg D_{H_2O}$, in agreement with conductivity data.[53]

TABLE VII. Inverse proton transfer rates, $1/k_1^{PT}$, and average lifetimes, τ_{exch}, of H^+(aq) and OH^-(aq) charge defects (all in ps) excluding rattling events.

Functional	Charge defect	$1/k_1^{PT}$	τ_{exch}
PW91	H^+(aq)	1.00	1.24
	OH^-(aq)	0.74	1.16
BLYP	H^+(aq)	1.68	1.66
	OH^-(aq)	3.20	3.20
HCTH	H^+(aq)	1.57	1.70
	OH^-(aq)	13.8	15.6

This paper presented a comprehensive prediction of charge transfer rates and defect lifetimes connected to structural diffusion of OH^-(aq) (see Sec. IV B) based on the dynamical hypercoordination mechanism, which has now been shown to be consistent with available experiments. By contrast, both the static hypercoordination and mirror image mechanisms fail qualitatively. The experimental database for this assessment includes isotopic substitution neutron scattering,[75,76,89–91] x-ray diffraction,[67] Fourier transform IR,[92,93] x-ray absorption spectroscopy,[94] core-level photoelectron spectroscopy,[95] femtosecond pump-probe vibrational spectroscopy,[77] two-dimensional IR,[77] and electrochemical conductivity measurements[53] as reviewed in detail in Ref. 8. The data compiled in Table VII show that the mirror image mechanism (PW91) leads to a situation where sustained PT (affecting net charge defect displacements and thus structural diffusion) is faster and the lifetime of the charge defect between true migration events (where trivial proton rattling is excluded) is shorter for OH^-(aq) in comparison with H^+(aq). The other extreme is static hypercoordination (HCTH) where the reverse is found: The lifetime of a given OH^-(aq) complex is exceedingly long compared to that of H^+(aq) and thus PT is expected to be extremely slow for OH^-(aq). Finally, dynamical hypercoordination (BLYP) predicts that the average lifetime of the OH^-(aq) solvation complexes is longer in comparison to H^+(aq) and thus that PT is slower in dilute basic solutions than in acids. The reported rates and time scales of elementary processes underlying charge migration in aqueous basic solutions should be most directly accessible by time-resolvent experiments, such as ultrafast spectroscopies, and are intended to serve as stimuli and predictions for deeper future analyses.

V. CONCLUSIONS AND OUTLOOK: TIME SCALES AS BENCHMARKS FOR MECHANISTIC PROPOSALS

A general statistical mechanical theory for analyzing and quantifying proton transfer and charge migration kinetics in hydrogen bond networks based on molecular dynamics trajectories has been introduced. Extending population correlation functions to identify distinct solvation-shell topologies, a chemical master equation framework is proposed from which rates and lifetimes can be obtained when applied to

trajectories. Within the same framework an integral equation formalism is shown to connect various popular types of these correlation functions.

Using this approach a comprehensive analysis of reorientational, hydrogen bond, solvation-shell, proton rattling, proton transfer, rotational relaxation, and structural diffusion time scales has been performed for both H^+(aq) and OH^-(aq), relevant to acidic and basic aqueous solutions, based on three widely used density functionals (PW91, BLYP, and HCTH). For H^+(aq), all functionals not only predict the same diffusion mechanism but also similar time scales for proton rattling, hydrogen bond relaxation, and structural diffusion, which are furthermore consistent with experimental data on the femtosecond and picosecond time scales. For OH^-(aq), however, they all yield qualitatively different mechanisms including vastly different time scales and rates. By virtue of an in-depth comparison of the simulated scenarios extracted from diffraction and spectroscopic experiments the so-called dynamical hypercoordination mechanism is shown to be consistent with all available data in stark contrast to the other proposals, i.e., mirror image and static hypercoordination scenarios. Since the associated time scales can be connected to qualitatively different charge migration mechanisms, experimental relaxation times, rates, and lifetimes are proposed to serve as benchmarks for checking the mechanistic proposals more directly using time-resolved experimental probes in the future. As an aside it is added that these differences in predicted mechanisms and time scales are clearly shown not to be related to the particular algorithm used to perform *ab initio* molecular dynamics, i.e., Car–Parrinello versus Born–Oppenheimer propagation, contrary to what has been suggested in the literature.

Last but not least, the study suggests that experiments on the *dynamics* would also provide insights into the solvation-shell *structure* of OH^-(aq) since both aspects have been shown to be intimately connected via the migration *mechanism* in conjunction with the predicted time scales and rates. Research along these lines is expected to pave exciting novel avenues to understand proton transfer reaction dynamics and charge migration *kinetics* not only in bulk solution chemistry but also in molecular materials and biomolecular processes.

Obviously, this is only the first step into quantifying charge defect kinetics of OH^-(aq) in hydrogen-bonded networks that can be extended in various ways. First of all, the introduced formalism is both general and flexible so that it can be straightforwardly adapted to topological charge defects moving in lower-dimensional networks, e.g., along one-dimensional wires and two-dimensional surfaces or within confinements, restricted geometries, and porous media, by modifying the population correlation functions. In these cases, the hydrogen-bonding contacts with the environments must be properly included in the definition. Next, the formalism can be transferred from idealized acidic and basic aqueous bulk solutions, as studied here, to diverse molecular systems such as those inspired from materials science, e.g., charge-conducting polymers, or biology, e.g., charge diffusion close to cell membranes. Finally, the linear rate theory resulting in the (multi-)exponential decay of the correlation functions, and thus Debye-like relaxation, can be applied up to time scales of the order of 10 ps, which is the relevant time window on which the structural diffusion scenarios discussed here differ at the molecular level. The situation gets more involved beyond this molecular time scale, where nonlinear kinetic theories able to yield nonexponential relaxation behavior are called for. Drawing on the mathematical concept of fractional calculus, it is suggested in the Appendix that the proton transfer correlation functions, including the corresponding rate equations, can be "translated" from standard kinetics into fractional kinetics, which have been used to describe "anomalous" diffusion (in the sense of non-Einsteinian diffusion) in, for example, supercooled liquids and glasses. In the case of proton migration in water, as shown in the Appendix, the resulting intermittent/history-independent correlation function turns out to be a superposition of two Mittag–Leffler (ML) functions, which are able to describe both exponential decay on the molecular time scale and power law decay $\sim t^{-3/2}$ at long-times. Recalling that the present investigation is based on about half a nanosecond of *ab initio* molecular dynamics simulations in total, it will be most interesting to explore fractional kinetics in future such long-time simulations of structural diffusion in water to find out how well such fractional kinetics can describe data spanning several orders of magnitude in time.

ACKNOWLEDGMENTS

Partial financial support is gratefully acknowledged as follows. M.E.T.: NSF Grant No. CHE-0704036 and the Alexander von Humboldt Foundation (AvH) for the Bessel Award 2005 that allowed stays as a Visiting Professor in Bochum; A.C.: Department of Science and Technology (DST), Department of Atomic Energy (DAE), and Council of Scientific and Industrial Research (CSIR), all Government of India, and Alexander von Humboldt Foundation (AvH) for a Fellowship that allowed stays as a Visiting Professor in Bochum; D.M.: Ruhr-Universität Bochum (RUB), Deutsche Forschungsgemeinschaft (DFG), and Fonds der Chemischen Industrie (FCI). The calculations were performed on Linux Clusters granted to A.C. by DST, DAE, CSIR, and AvH Foundation as well as at Bovilab@RUB (Bochum) and Rechnerverbund-NRW. In addition, we are most grateful to Rudolf Hilfer for providing us with numerical data of the Mittag–Leffler functions used to compute the intermittent correlation function depicted in Fig. 10 of Appendix.

APPENDIX: FRACTIONAL KINETICS AS A POSSIBLE MODEL FOR LONG-TIME DECAY

The simple linear rate theory defined by the chemical master equation formalism in Eqs. (8) and (10) yields a multiexponential decay of the intermittent PT correlation functions. Such a decay pattern is reasonable for short and intermediate times but is likely not correct for the long-time decay of these functions, where a power law decay of the form $t^{-\sigma}$, where σ is, in general, a fractional power. When this long-time decay is dominated by three-dimensional diffusional dynamics,[44] $\sigma=3/2$. A linear kinetic theory will never be capable of yielding such decay. In order to allow for such algebraic decay on long-time scales, it is necessary to

weaken the depletion of A^* and generation of A' connected with the $d[A^*](t)/dt$ in Eqs. (7) and (9) and similarly for the depletion of A' and generation of A^* connected with the $d[A'](t)/dt$.

An interesting mechanism for achieving this is through the use of fractional kinetics,[96–100] which is based on the fractional calculus.[101] In this section, we propose one possible fractional kinetic model to replace the linear chemical master equation in Eqs. (8) and (10). We will show that a more general time dependence of the decay properties of various correlation functions can be achieved with the addition of just one or possibly two additional parameters. Although the physical justification for such a model is not entirely clear at present, we will suggest a possible reason for weakening the linear terms in the kinetic model. We will begin with a brief review of the fractional calculus, and we will then present the new kinetic model and derive its solution.

Our review of the fractional calculus begins with a generalization of the formula for the nth derivative of a power m of a variable x,

$$\frac{d^n}{dx^n}x^m = \frac{m!}{(n-m)!}x^{m-n}. \tag{A1}$$

If we wish to generalize this formula to an arbitrary, possibly noninteger power μ of x and a noninteger order γ of differentiation, the formula in Eq. (A1) can be generalized via introduction of the gamma function

$$\Gamma(y) = \int_0^\infty t^{y-1}e^{-t}dt. \tag{A2}$$

Using the gamma function, we define the fractional Riemann–Liouville derivative of order $\gamma \leq \mu$ as

$$\frac{d^\gamma}{dx^\gamma}x^\mu = \frac{\Gamma(\mu+1)}{\Gamma(\mu-\gamma+1)}x^{\mu-\gamma}. \tag{A3}$$

These simple ideas can be generalized to define an operator for fractional differentiation and integration (i.e., antidifferentiation or differentiation using a negative order) of an arbitrary function $f(x)$. We define the fractional integral of $f(x)$ at arbitrary order γ via

$${}_aD_x^{-\gamma}f(x) = \frac{1}{\Gamma(\gamma)}\int_a^x (x-y)^{\gamma-1}f(y)dy. \tag{A4}$$

The fractional derivative operator ${}_aD_x^\gamma$ is then defined using the fractional integration operator as

$${}_aD_x^\gamma = \frac{d^n}{dx^n}{}_aD_x^{\gamma-n}, \tag{A5}$$

where $n > \gamma$ and $n = \text{int}(\gamma)+1$.

Now consider the Laplace transform of the quantity

$$g(t) = {}_0D_t^{-\gamma}f(t). \tag{A6}$$

Using Eq. (A4), this Laplace transform becomes

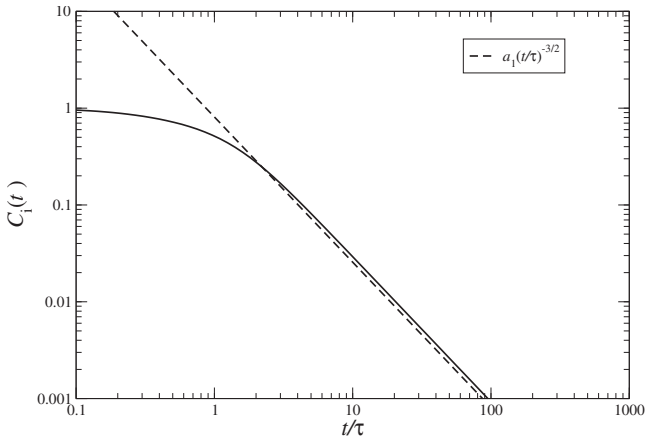

FIG. 10. Double-logarithmic plot of the intermittent correlation function according to Eq. (A18) using the following model parameters: $\alpha = 1/2$, $\sigma = \alpha+1$, $a_0 = 1$, and $\tau_1 = \tau = 1$; the underlying Mittag–Leffler function was kindly generated by Hilfer according to Ref. 105. The asymptotic form $C_i(t) \to t^{-3/2}$ is shown in the red line. Compare the behavior of $C_i(t)$ to Fig. 6 of Ref. 44.

$$\tilde{g}(s) = \frac{1}{\Gamma(\gamma)}\int_0^\infty dte^{-st}\int_0^t (t-\tau)^{\gamma-1}f(\tau)d\tau. \tag{A7}$$

Making use of the convolution theorem for Laplace transforms, Eq. (A7) can be rewritten as

$$\tilde{g}(s) = \tilde{f}(s)\frac{1}{\Gamma(\gamma)}\int_0^\infty dte^{-st}t^{\gamma-1}. \tag{A8}$$

If we now introduce the change of variables $u = st$ into Eq. (A8), we obtain

$$\tilde{g}(s) = \frac{\tilde{f}(s)}{s}\frac{1}{\Gamma(\gamma)}\int_0^\infty due^{-u}\left(\frac{u}{s}\right)^{\gamma-1}$$

$$= \tilde{f}(s)s^{-\gamma}\frac{1}{\Gamma(\gamma)}\int_0^\infty due^{-u}u^{\gamma-1} = s^{-\gamma}\tilde{f}(s). \tag{A9}$$

We, therefore, have the Laplace transform relation

$$\int_0^\infty dte^{-st}{}_0D_t^{-\gamma}f(t) = s^{-\gamma}\tilde{f}(s), \tag{A10}$$

which will be key for the solution of our proposed kinetic model.

We now propose a modification of the linear theory for obtaining the PT correlation functions according to Eqs. (8) and (10) by the introduction of the fractional integration/differentiation operator as a means of weakening the depletion and generation of the species A' and A^*. In particular, suppose we replace Eqs. (8) and (10) with

$$\frac{dC_i(t)}{dt} = -\kappa_1^{PT}{}_0D_t^{-(\alpha-1)}C_i(t) + \kappa_{-1}^{PT}{}_0D_t^{-(\alpha-1)}C_{nn}(t),$$

$$\frac{dC_{nn}(t)}{dt} = -(\kappa_2^{PT}+\kappa_{-1}^{PT})_0D_t^{-(\alpha-1)}C_{nn}(t) + \kappa_1^{PT}{}_0D_t^{-(\alpha-1)}C_i(t), \tag{A11}$$

where α is the fractional order to be fit to the correlation function data, and where each of the new rate constants κ is

simply k^α, with k being the original rate constants in Eqs. (8) and (10). As in the original chemical master equation, these must be solved subject to the initial conditions $C_i(0)=1$ and $C_{nn}(0)=0$. Note that Eq. (A11) adds one additional parameter, namely, the exponent α, to the kinetic model.

This model can be solved by taking the Laplace transform of both sides and solving the algebraic equations for $\tilde{C}_i(s)$ and $\tilde{C}_{nn}(s)$. Using Eq. (A10), this procedure gives for $\tilde{C}_i(s)$

$$\begin{aligned}\tilde{C}_i(s) &= \frac{s+Ks^{-(\alpha-1)}}{(s+\kappa_1^{PT}s^{-(\alpha-1)})(s+Ks^{-(\alpha-1)})-\kappa_1^{PT}\kappa_{-1}^{PT}s^{-2(\alpha-1)}} \\ &= \frac{s+Ks^{-(\alpha-1)}}{s^2+(\kappa_1^{PT}+K)ss^{-(\alpha-1)}+\kappa_1^{PT}(K-\kappa_{-1}^{PT})s^{-2(\alpha-1)}} \\ &= \frac{1}{s}\left\{\frac{1+Ks^{-\alpha}}{1+(\kappa_1^{PT}+K)s^{-\alpha}+\kappa_1^{PT}(K-\kappa_{-1}^{PT})s^{-2\alpha}}\right\}, \quad \text{(A12)}\end{aligned}$$

where $K=\kappa_2^{PT}+\kappa_{-1}^{PT}$. This Laplace transform can be inverted analytically using the fact that the inverse of $1/s(1-\lambda s^{-\alpha})$ is $E_\alpha(\lambda t^\alpha)$, where $E_\alpha(z)$ is the Mittag-Leffler (ML) function[102,103]

$$E_\alpha(z)=\sum_{k=0}^{\infty}\frac{z^k}{\Gamma(\alpha k+1)}. \quad \text{(A13)}$$

ML functions are often referred to as "generalized" exponentials with the $\Gamma(\alpha k+1)$ denominator in Eq. (A13) representing a generalization of the factorial that appears in the Taylor expansion of $\exp(z)$. By expressing Eq. (A12) in terms of partial fractions of the form

$$\begin{aligned}&\frac{1+Ks^{-\alpha}}{1+(\kappa_1^{PT}+K)s^{-\alpha}+\kappa_1^{PT}(K-\kappa_{-1}^{PT})s^{-2\alpha}} \\ &\quad = \frac{A}{1+as^{-\alpha}}+\frac{B}{1+bs^{-\alpha}}, \quad \text{(A14)}\end{aligned}$$

where A, B, a, b are determined such that Eq. (A14) is an equality.

When this is done, we obtain for the relevant intermittent PT correlation function a form similar to Eq. (14) but with ML functions replacing the exponentials,

$$\begin{aligned}C_i(t) &= \frac{1}{2\lambda}[(\lambda-k_1^{PT}+K)E_\alpha(-(t/\tau_1)^\alpha) \\ &\quad +(\lambda+k_1^{PT}-K)E_\alpha(-(t/\tau_2)^\alpha)], \quad \text{(A15)}\end{aligned}$$

where

$$\lambda=\sqrt{(\kappa_1^{PT}-K)^2+4\kappa_1^{PT}\kappa_{-1}^{PT}} \quad \text{(A16)}$$

and

$$\begin{aligned}\tau_1 &= \left(\frac{2}{\kappa_1^{PT}+K-\lambda}\right)^{-1/\alpha}, \\ \tau_2 &= \left(\frac{2}{\kappa_1^{PT}+K+\lambda}\right)^{-1/\alpha}, \quad \text{(A17)}\end{aligned}$$

which is the crucial result of this analysis. The significance of the form obtained in Eq. (A15) is that the ML functions, for short times, behave like stretched exponentials, $E_\alpha(-(t/\tau)^\alpha)\approx\exp(-(t/\tau)^\alpha)/\Gamma(1+\alpha)$. If $\alpha=1$, $E_\alpha(-(t/\tau)^\alpha)=\exp(-t/\tau)$, and the fractional kinetic model reverts to the linear kinetic model of Eq. (14). For noninteger α, because $-1=\exp(i\pi)$, the phase of the arguments of the ML functions is π, and the asymptotic behavior of the ML functions is $E_\alpha(-(t/\tau)^\alpha)\to(t/\tau)^{-\alpha}/\Gamma(1-\alpha)$. For example, if $\alpha=1/2$, at long-times $E_{1/2}(-(t/\tau)^{1/2})\sim(t/\tau)^{-1/2}$ is found, which would accord with a one-dimensional diffusion model.

An alternative to Eq. (A15) would allow the order of the ML function and the exponent in the argument to differ, i.e., we choose ML functions of the form $E_\alpha(-(t/\tau)^\sigma)$, where $\sigma>\alpha$ in order to model the decay of the correlation functions in more than one dimension. These functions would enter the intermittent/history-independent correlation function $C_i(t)$ as

$$C_i(t)=a_0E_\alpha(-(t/\tau_1)^\sigma)+(1-a_0)E_\alpha(-(t/\tau_2)^\sigma), \quad \text{(A18)}$$

with a_0, τ_1, τ_2, α, and σ as fitting parameters, instead of a_0, $\tau_1=1/a_1$, and $\tau_2=1/a_2$ in Eq. (16). A set of underlying kinetic equations yielding Eq. (A18) is nontrivial and will be reserved for a future study. However, as an example, if $\alpha=1/2$ and $\sigma=\alpha+1$, the long-time behavior would go as $\sim(t/\tau)^{-3/2}$ in accord with a three-dimensional diffusional picture.[44] However, the AIMD trajectories used to generate the PT correlation functions in Eqs. (1), (2), and (4) are not long enough to reveal this long-time behavior. As was demonstrated in Sec. IV we find that we can fit the data satisfactorily with the multiexponential forms of the previous section out to times for which the values of $C_i(t)$ and $C_c(t)$ are well below one-tenth of their initial values. Recalling the discussion at the end of the previous Sec. II A, it was shown in Ref. 44, based on empirical valence bond MD, that the biexponential form of PT correlation functions describes proton migration kinetics accurately up to 30 ps whereas significant relative deviations are seen only on the time scale of $\sim$100 ps in a log-log representation. Nevertheless, it is interesting to consider the behavior of Eq. (A.18) for model data, as depicted in Fig. 10. The figure shows a log-log plot of $C_i(t)$ together with the asymptotic form $\sim t^{-3/2}$. Thus, by generalizing the exponentials in the multiexponential form of the previous section with the ML functions, better fits to the long-time behavior of the correlation functions generated from MD trajectories might be possible. This analysis shows an intriguing application of the fractional kinetics framework. We note, in passing, that efficient algorithms for generating ML functions[104] were recently introduced by Seybold and Hilfer[105] and a detailed description of the mathematical properties of ML functions can be found in Refs. 102 and 103.

Interestingly, applying the integral equation theory of Sec. II B, if the correlation functions are represented by single ML functions $C_c(t)\sim E_\alpha(-\lambda_1 t^\alpha)$ and $N_c(t)\sim E_\alpha(-\lambda_2 t^\alpha)$, then Eq. (38) yields $C_i(t)\sim E_\alpha(-(\lambda_1+\lambda_2)t^\alpha)$. The same holds when $C_c(t)\sim E_\alpha(-\lambda_1 t^\sigma)$ and $N_c(t)\sim E_\alpha(-\lambda_2 t^\sigma)$. Although we have not shown it, we expect the same types of relations hold for multi-ML forms for $C_c(t)$ and $N_c(t)$.

[1] F. H. Stillinger, in *Theoretical Chemistry: Advances and Perspectives*, edited by H. Eyring and D. Henderson (Academic, New York, 1978), pp. 177–234.
[2] M. Eigen, Angew. Chem., Int. Ed. Engl. **3**, 1 (1964).
[3] K. D. Kreuer, S. J. Paddison, E. Spohr, and M. Schuster, Chem. Rev. (Washington, D.C.) **104**, 4637 (2004).
[4] M. Schuster, W. H. Meyer, G. Wegner, H. G. Herz, M. Ise, M. Schuster, K. D. Kreuer, and J. Maier, Solid State Ionics **110**, 85 (2001).
[5] D. A. Boysen, T. Uda, C. R. I. Chisholm, and S. M. Haile, Science **303**, 68 (2004).
[6] C. A. Wraight, Biochim. Biophys. Acta **1757**, 886 (2006).
[7] M. Tuckerman, A. Chandra, and D. Marx, Acc. Chem. Res. **39**, 151 (2006).
[8] D. Marx, A. Chandra, and M. E. Tuckerman, Chem. Rev. (Washington, D.C.) **110**, 2174 (2010).
[9] D. Marx, ChemPhysChem **7**, 1848 (2006); **8**, 209 (2007).
[10] G. A. Voth, Acc. Chem. Res. **39**, 143 (2006).
[11] B. Roux, Acc. Chem. Res. **35**, 366 (2002).
[12] M. E. Tuckerman, K. Laasonen, M. Sprik, and M. Parrinello, J. Phys.: Condens. Matter **6**, A93 (1994).
[13] M. E. Tuckerman, K. Laasonen, M. Sprik, and M. Parrinello, J. Chem. Phys. **103**, 150 (1995).
[14] M. E. Tuckerman, K. Laasonen, M. Sprik, and M. Parrinello, J. Phys. Chem. **99**, 5749 (1995).
[15] M. Tuckerman, D. Marx, and M. Parrinello, Nature (London) **417**, 925 (2002).
[16] A. Chandra, M. E. Tuckerman, and D. Marx, Phys. Rev. Lett. **99**, 145901 (2007).
[17] H. J. Bakker and H. K. Nienhuys, Science **297**, 587 (2002).
[18] M. Rini, B. Z. Magnes, E. Pines, and E. T. J. Nibbering, Science **301**, 349 (2003).
[19] O. F. Mohammed, D. Pines, J. Dreyer, E. Pines, and E. T. J. Nibbering, Science **310**, 83 (2005).
[20] S. Woutersen and H. J. Bakker, Phys. Rev. Lett. **96**, 138305 (2006).
[21] W. Amir, G. Gallot, F. Hache, S. Bratos, J.-C. Leicknam, and R. Vuilleumier, J. Chem. Phys. **126**, 034511 (2007).
[22] D. B. Spry, A. Goun, and M. D. Fayer, J. Phys. Chem. A **111**, 230 (2007).
[23] O. F. Mohammed, D. Pines, E. T. J. Nibbering, and E. Pines, Angew. Chem., Int. Ed. **46**, 1458 (2007).
[24] D. B. Spry and M. D. Fayer, J. Chem. Phys. **128**, 084508 (2008).
[25] K. J. Tielrooij, R. L. A. Timmer, H. J. Bakker, and M. Bonn, Phys. Rev. Lett. **102**, 198303 (2009).
[26] D. T. Gillespie, Physica A **188**, 404 (1992).
[27] S. Peleš, B. Munsky, and M. Khammash, J. Chem. Phys. **125**, 204104 (2006).
[28] D. T. Gillespie, Annu. Rev. Phys. Chem. **58**, 35 (2007).
[29] T. Jahnke and W. Huisinga, J. Math. Biol. **54**, 1 (2007).
[30] F. H. Stillinger, Adv. Chem. Phys. **31**, 1 (1975).
[31] D. C. Rapaport, Mol. Phys. **50**, 1151 (1983).
[32] D. Chandler, *Introduction to Modern Statistical Mechanics* (Oxford University Press, Oxford, 1987).
[33] A. Luzar and D. Chandler, Phys. Rev. Lett. **76**, 928 (1996).
[34] A. Luzar and D. Chandler, Nature (London) **379**, 55 (1996).
[35] A. Luzar, J. Chem. Phys. **113**, 10663 (2000).
[36] A. Chandra, Phys. Rev. Lett. **85**, 768 (2000).
[37] S. Balasubramanian, S. Pal, and B. Bagchi, Phys. Rev. Lett. **89**, 115505 (2002).
[38] E. Schreiner, C. Nicolini, B. Ludolph, R. Ravindra, N. Otte, A. Kohlmeyer, R. Rousseau, R. Winter, and D. Marx, Phys. Rev. Lett. **92**, 148101 (2004).
[39] R. Rousseau, E. Schreiner, A. Kohlmeyer, and D. Marx, Biophys. J. **86**, 1393 (2004).
[40] D. Laage and J. T. Hynes, Science **311**, 832 (2006).
[41] D. Laage and J. T. Hynes, J. Phys. Chem. B **112**, 14230 (2008).
[42] J. A. Morrone, K. E. Haslinger, and M. E. Tuckerman, J. Phys. Chem. B **110**, 3712 (2006).
[43] D. Marx and J. Hutter, *Ab Initio Molecular Dynamics: Basic Theory and Advanced Methods* (Cambridge University Press, Cambridge, 2009).
[44] H. Chen, G. A. Voth, and N. Agmon, J. Phys. Chem. B **114**, 333 (2010).
[45] D. Laage and J. Hynes, J. Phys. Chem. B **112**, 7697 (2008).
[46] I. Ohmine and H. Tanaka, Chem. Rev. (Washington, D.C.) **93**, 2545 (1993).
[47] O. Markovitch and N. Agmon, J. Chem. Phys. **129**, 084505 (2008).
[48] N. Agmon, Chem. Phys. Lett. **319**, 247 (2000).
[49] R. Ludwig, Angew. Chem., Int. Ed. **42**, 258 (2003).
[50] Z. Zhu and M. E. Tuckerman, J. Phys. Chem. B **106**, 8009 (2002).
[51] D. Asthagiri, L. R. Pratt, J. D. Kress, and M. A. Gomez, Chem. Phys. Lett. **380**, 530 (2003).
[52] D. Asthagiri, L. R. Pratt, J. D. Kress, and M. A. Gomez, Proc. Natl. Acad. Sci. U.S.A. **101**, 7229 (2004).
[53] P. Atkins and J. de Paula, *Atkins' Physical Chemistry*, 8th ed. (Oxford University Press, Oxford, 2006).
[54] N. Agmon, Chem. Phys. Lett. **244**, 456 (1995).
[55] D. Marx, Science **303**, 634 (2004).
[56] D. Marx, M. E. Tuckerman, J. Hutter, and M. Parrinello, Nature (London) **397**, 601 (1999).
[57] H. Lapid, N. Agmon, M. K. Petersen, and G. A. Voth, J. Chem. Phys. **122**, 014506 (2005).
[58] O. Markovitch, H. Chen, S. Izvekov, F. Paesani, G. A. Voth, and N. Agmon, J. Phys. Chem. B **112**, 9456 (2008).
[59] A. Eucken, Z. Elektrochem. Angew. Phys. Chem. **52**, 255 (1948).
[60] A. Gierer and K. Wirtz, Ann. Phys. **6**, 257 (1949).
[61] T. C. Berkelbach, H. S. Lee, and M. E. Tuckerman, Phys. Rev. Lett. **103**, 238302 (2009).
[62] A. D. Becke, Phys. Rev. A **38**, 3098 (1988).
[63] C. Lee, W. Yang, and R. G. Parr, Phys. Rev. B **37**, 785 (1988).
[64] A. D. Boese, N. L. Doltsinis, and N. C. Handy, J. Chem. Phys. **112**, 1670 (2000).
[65] J. P. Perdew and Y. Wang, Phys. Rev. B **45**, 13244 (1992).
[66] P. Vassilev, M. J. Louwerse, and E. J. Baerends, J. Phys. Chem. B **109**, 23605 (2005).
[67] T. Megyes, S. Balint, T. Grosz, T. Radnai, I. Bakó, and P. Sipos, J. Chem. Phys. **128**, 044501 (2008).
[68] J. P. Renault, R. Vuilleumier, and S. Pommeret, J. Phys. Chem. A **112**, 7027 (2008).
[69] R. Car and M. Parrinello, Phys. Rev. Lett. **55**, 2471 (1985).
[70] D. Marx and J. Hutter, in *Modern Methods and Algorithms of Quantum Chemistry*, NIC Series, edited by J. Grotendorst (Forschungszentrum, Juelich, 2000), Vol. 1.
[71] M. E. Tuckerman, J. Phys.: Condens. Matter **14**, R1297 (2002).
[72] J. Hutter, A. Alavi, T. Deutsch, M. Bernasconi, S. Goedecker, D. Marx, M. Tuckerman and M. Parrinello, CPMD, IBM Corporation 1990–2009 and MPI für Festkörperforschung 1997–2001; see www.cpmd.org, 2009.
[73] C. J. Fecko, J. J. Loparo, S. T. Roberts, and A. Tokmakoff, J. Chem. Phys. **122**, 054506 (2005).
[74] H. K. Nienhuys, A. J. Lock, R. A. van Santen, and H. J. Bakker, J. Chem. Phys. **117**, 8021 (2002).
[75] A. Botti, F. Bruni, S. Imberti, M. A. Ricci, and A. K. Soper, J. Chem. Phys. **120**, 10154 (2004).
[76] S. E. McLain, S. Imberti, A. K. Soper, A. Botti, F. Bruni, and M. A. Ricci, Phys. Rev. B **74**, 094201 (2006).
[77] S. T. Roberts, P. B. Petersen, K. Ramasesha, A. Tokmakoff, I. S. Ufimtsev, and T. J. Martinez, Proc. Natl. Acad. Sci. U.S.A. **106**, 15154 (2009).
[78] G. Gallot, S. Bratos, S. Pommeret, N. Lascoux, J.-C. Leicknam, M. Kozinski, W. Amir, and G. M. Gale, J. Chem. Phys. **117**, 11301 (2002).
[79] J. Thøgersen, S. K. Jensen, C. Petersen, and S. R. Keiding, Chem. Phys. Lett. **466**, 1 (2008).
[80] C. Petersen, J. Thøgersen, S. K. Jensen, and S. R. Keiding, J. Phys. Chem. A **111**, 11410 (2007).
[81] S. Park and M. D. Fayer, Proc. Natl. Acad. Sci. U.S.A. **104**, 16731 (2007).
[82] D. E. Moilanen, E. E. Fenn, Y.-S. Lin, J. L. Skinner, B. Bagchi, and M. D. Fayer, Proc. Natl. Acad. Sci. U.S.A. **105**, 5295 (2008).
[83] Y. L. A. Rezus and H. J. Bakker, J. Chem. Phys. **123**, 114502 (2005).
[84] D. Cringus, S. Yeremenko, M. S. Pshenichnikov, and D. A. Wiersma, J. Phys. Chem. B **108**, 10376 (2004).
[85] T. W. N. Bieze, J. R. C. van der Maarrel, and J. C. Leyte, Chem. Phys. Lett. **216**, 56 (1993).
[86] R. Ludwig, Chem. Phys. **195**, 329 (1995).
[87] X. Q. Sun, S. Yoo, S. S. Xantheas, and L. X. Dang, Chem. Phys. Lett. **481**, 9 (2009).
[88] B. S. Mallik and A. Chandra, J. Mol. Liq. **143**, 31 (2008).
[89] A. Botti, F. Bruni, S. Imberti, M. A. Ricci, and A. K. Soper, J. Chem. Phys. **119**, 5001 (2003).
[90] S. Imberti, A. Botti, F. Bruni, G. Cappa, M. A. Ricci, and A. K. Soper, J. Chem. Phys. **122**, 194509 (2005).
[91] A. Botti, F. Bruni, S. Imberti, M. A. Ricci, and A. K. Soper, J. Mol. Liq.

117, 81 (2005).
[92] M. Śmiechowski and J. Stangret, J. Phys. Chem. A **111**, 2889 (2007).
[93] M. Śmiechowski and J. Stangret, J. Mol. Struct. **834–836**, 239 (2007).
[94] C. D. Cappa, J. D. Smith, B. M. Messer, R. C. Cohen, and R. J. Saykally, J. Phys. Chem. A **111**, 4776 (2007).
[95] E. F. Aziz, N. Ottosson, M. Faubela, I. V. Hertel, and B. Winter, Nature (London) **455**, 89 (2008).
[96] R. Hilfer and L. Anton, Phys. Rev. E **51**, R848 (1995).
[97] R. Hilfer, Fractals **3**, 549 (1995).
[98] R. Metzler and J. Klafter, Phys. Rep. **339**, 1 (2000).
[99] R. Hilfer, J. Phys. Chem. B **104**, 3914 (2000).
[100] I. M. Sokolov, J. Klafter, and A. Blumen, Phys. Today **55**(11), 48 (2002).
[101] *Applications of Fractional Calculus in Physics*, edited by R. Hilfer (World Scientific, Singapore, 2000).
[102] A. K. Shukla and J. C. Prajapati, J. Math. Anal. Appl. **336**, 797 (2007).
[103] H. J. Haubold, A. M. Mathai, and R. K. Saxena, e-print arXiv:0909.0230.
[104] R. Hilfer and H. J. Seybold, Integral Transforms Spec. Funct. **17**, 637 (2006).
[105] H. Seybold and R. Hilfer, SIAM (Soc. Ind. Appl. Math.) J. Numer. Anal. **47**, 69 (2008).